TU

TECHNISCHE UNIVERSITÄT WIEN

DISSERTATION

Advection-dominated Models for Chemotaxis

ausgeführt zum Zwecke der Erlangung des akademischen Grades eines
Doktors der technischen Wissenschaften unter der Leitung von

Ao. Univ. Prof. Dr. techn. Christian Schmeiser
Institut für Analysis und Scientific Computing (E101)

eingereicht an der Technischen Universität Wien
Fakultät für Mathematik und Geoinformation

von

Dipl.Ing. Yasmin Dolak
Matr. Nr. 9526063
Schopenhauerstraße 15/10
1180 Wien

Wien, am 12. Oktober 2004

Kurzfassung

Die vorliegende Arbeit beschäftigt sich mit mathematischen Modellen für Chemotaxis, der gerichteten Bewegung von Organismen, die durch chemische Substanzen ausgelöst und gelenkt wird. Chemotaxis spielt für viele biologische und physiologische Prozesse eine entscheidende Rolle, angefangen bei Wundheilung oder der Reaktion unseres Immunsystems bis zu Embryogenese und der Bildung neuer Blutgefäße. Zahlreiche Mikroorganismen benützen Chemotaxis, um Nahrung aufzuspüren oder toxische Substanzen zu vermeiden.

Während bei der chemotaktischen Orientierung von Bakterien die ungerichtete, zufällige Komponente ihrer Bewegung eine wichtige Rolle spielt, unterdrücken andere Organismen, zum Beispiel zelluläre Schleimpilze, die Zufallsbewegungen größtenteils, was zu einer sehr zielgerichteten Fortbewegung führt.

In einem mathematischen Modell kann letzteres auf mehrere Arten ausgedrückt werden. In einem sogenannten makroskopischen Modell wird die zeitliche Veränderung der Zelldichte durch Diffusion und Advektion bestimmt - wird Zufallsbewegung unterdrückt, so dominiert der Advektionsterm.

Ein anderer Ansatz, Zellbewegung zu modellieren kommt ursprünglich aus der Gasdynamik: in einer kinetischen Transportgleichung werden Richtungswechsel der Zellen durch einen Integraloperator beschrieben. Dominiert die zielgerichtete Bewegung der Zellen, so legen die führenden Terme dieses Integraloperators die Orientierung am Gradienten fest (im Falle, dass der Anteil der ungerichteten Bewegung überwiegt, beschreiben die führenden Terme Bewegungsänderungen ohne bevorzugte Richtung). Beide Modellierungsansätze werden in dieser Arbeit behandelt.

Im ersten Teil präsentieren wir ein kinetisches Modell für Chemotaxis das auf der Annahme basiert, dass die Zellen Konzentrationsunterschiede entlang ihres Weges messen und vergleichen. Nach einer passenden Skalierung des Problems untersuchen wir den makroskopische Limes für dieses Modell. In erster Ordnung erhalten wir eine reine Konvektionsgleichung für die Zelldichte, als Korrektur höherer Ordnung wird ein Diffusionsterm hergeleitet. Als Anwendungsbeispiel untersuchen wir das Verhalten des Schleimpilzes *Dictyostelium discoideum*. Die numerische Lösung der Gleichungen zeigt, dass unser Modell einen erfolgreichen Erklärungsansatz für das so genannte chemotaktische Paradoxon darstellt.

Im zweiten Teil der Arbeit untersuchen wir ein makroskopisches Advektions-Diffusions Modell für Chemotaxis. Dieses Modell berücksichtigt die endliche Größe der Zellen: ein Sättigungsterm im chemotaktischen Fluss verhindert, dass die Zelldichte beliebig hoch wird. Wir betrachten die Gleichungen für den Fall einer kleinen Diffusivität und zeigen, dass Lösungen des vollen Pro-

blems gegen Lösungen der reinen Advektionsgleichung konvergieren wenn die Diffusionskonstante gegen Null geht. Für kleine, positive Diffusivität zeigen Lösungen ein interessantes Langzeitverhalten: durch den nichtlinearen Advektionsterm bilden Lösungen plateau-artige Strukturen, die lange, stabile Perioden aufweisen, die immer wieder von schnellen Übergängen unterbrochen werden, während denen einzelne Plateaus miteinander verschmelzen. Wir wenden Methoden der formalen Asymptotik an, um ein System von gewöhnlichen Differentialgleichungen herzuleiten, die die Bewegung der Plateaus beschreiben.

Acknowledgement

Contents

Chapter 1

Introduction

How do predators such as sharks or snakes detect their prey? How can male silk moths find the females that are willing to mate? How do the white blood cells in our immune system locate the sites of infection? The answer is always the same: they are guided by chemical cues from their environment. And whether we think of the growth of new blood vessels, wound healing or embryogenesis - many basic processes in our body depend on the ability of cells to orient on chemical gradients. In this thesis, we will be concerned with the mathematical modelling of this phenomenon. In particular, we will investigate models arising if the random component of cell motion is small compared to the active, directed movement of cells. After a brief introduction on the biological and mathematical background, we will derive kinetic models for chemotaxis and investigate their macroscopic limit. In the second half of the thesis, we will study a macroscopic model for chemotaxis with small diffusion and investigate the limit of vanishing diffusivity. A more specific introduction into the subject will be given at the beginning of each chapter.

1.1 Biological background

Several different types of response to chemical stimuli have been classified (see for instance Fraenkel and Gunn [12]): whereas *chemokinesis* generally describes response without a directional component (a classical example are flagellated bacteria, changing their turning frequency according to concentration changes of the chemical substances in their environment), *chemotaxis* is used to describe the directed response of an individual to chemical gradients. If the attractant is an adhesion molecule bound to a substrate, the expression *haptotaxis* is used. However, a straightforward classification is not always possible. Because all these different mechanisms can lead to the same effects on the population level, for instance to aggregation at the site of maximal chemical concen-

tration, they are sometimes summarized into the term *chemosensitive movement* (for a more detailed discussion, see Hillen [17]). Nevertheless, the term *chemotaxis* is still widely used in the literature for all kinds of chemosensitive responses, and in the following, we will also use the word in this general sense.
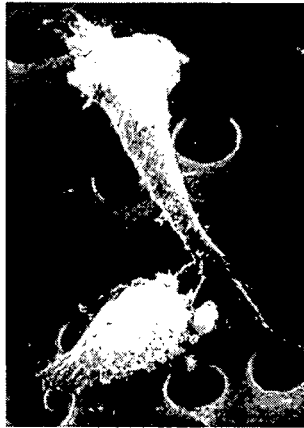
One of the best studied creatures displaying chemotactic behaviour is the slime mold* *Dictyostelium discoideum* (Dd), one of the model organisms chosen by the National Institutes of Health. The amoeba is easy to cultivate, has a fast reproduction rate, and its genome contains many genes that are homologous to those in higher eukaryotes. A whole range of molecular biological tools such as gene knockout or marker genes can be used with Dd (which is for instance not possible for end differentiated cells in humans such as neutrophils).

Most importantly, Dd is a fascinating example of how single cells can develop into a multicellular organism: Under normal conditions, the amebae live in the forest soil, feeding on bacteria. When starved, the cells develop the ability to produce and react to the messenger molecule cyclic adenosine monophosphate (cAMP), which also plays an important role in signal transduction in the human body. Randomly located cells called *pacemakers* produce the chemical in a periodic fashion, and cells around them begin to produce the chemical themselves, until a negative feedback loop shuts down the production again. In consequence, travelling pulses of cAMP in the form of concentric rings (*target patterns*) or spirals spread over the cell lawn [1]. Cells move towards the source of the chemical waves and consequently, aggregates of up to 10^5 cells are formed. Eventually, the aggregates (*mound*) topple over and become so-called *slugs*. A slug migrates on the substratum until a suitable place for the formation of a fruiting-body is found. Differentiation and sorting of cells already starts during the mound stage, and as the fruiting body is formed, cells in the forward end of the slug become stalk cells, and cells in the posterior end become spores. The stalk cells die and form the stalk of the fruiting body,

Figure 1.1: Two human neutrophils trying to squeeze through the pores of a filter in response to a chemoattractant diffusing up from beneath

---

*Once considered as fungi, slime molds are now counted among the kingdom of protista, which can be roughly described as unicellular eukaryotes (i.e. in contrast to bacteria, the cells have a true nucleus).

(a) Target patterns [31]

(b) Early aggregation stage [11]
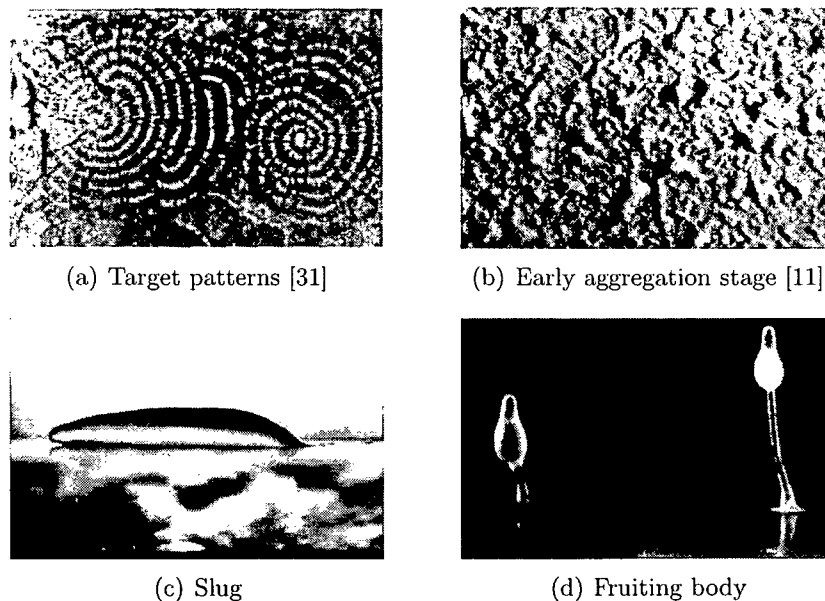

(c) Slug

(d) Fruiting body

Figure 1.2: Different stages of the life cycle of *Dictyostelium discoideum*

whereas the spore cells survive inside a spore cap until conditions for survival are favourable again. Then, the spore cap bursts open, each spore germinates into an amoeba, and the whole cycle can start anew (Figure 1.2). There also exists a sexual pathway controlled by chemotaxis, where two amoebae fuse with each other to form one single, large amoeba (*zygote*). Other cells are attracted to its surface by secretion of cAMP, and are endocytosed. When all surrounding amoebae are ingested, a cellulose wall develops around the greatly enlarged zygote. The zygote undergoes meiosis and progressive divisions, until germination takes place and a new generation of amoebae is released.

1.2   Mathematical modelling

Over the last decades, there has been a large number of attempts to describe chemotaxis mathematically. One of the earliest models for chemotaxis was introduced by Keller and Segel in 1970. In [27], the authors derive a system of four coupled reaction-diffusion equations, which is eventually reduced to a system of two equations for the cell density $\varrho(t, x)$ and the chemical concentration $S(t, x)$, depending on position $x \in \mathbb{R}^n$ and time $t \geq 0$:

$$\varrho_t + \nabla \cdot (k_1(\varrho, S)\nabla S - k_2(\varrho, S)\nabla \varrho) = 0, \qquad (1.1)$$

$$S_t = D_S \Delta S + k_3(\varrho, S). \qquad (1.2)$$

Almost the same equation for the cell density was derived by Patlak [40] in 1953 from a random walk problem. Nevertheless, the above equations have become mostly known as the Keller-Segel model for chemotaxis. Models based on this system have been successfully used to describe various phenomena based on chemotaxis, ranging from pigmentation patterns on fish skins [37] to embryogenesis [38].

Analytically, especially the case $k_1(\varrho, S) = \chi\varrho$, $k_3 = \varrho - S$ has been studied in great detail, and it turned out that for $\chi = const.$ and space dimension $n \geq 2$, solutions of (1.1), (1.2) can become unbounded in finite time. A large effort has been put into describing the *blow-up* of solutions and its preconditions - for a very comprehensive review, see Horstmann [24] and [25]. On the other hand, there have also been attempts to derive models preventing blow-up: In Hillen and Painter [21], global existence of solutions of (1.1), (1.2) with $k_1(\varrho, S) = \varrho\alpha(\varrho)\chi(S)$ and $k_3 = \beta(\varrho, S)\varrho - \gamma(\varrho, S)S$ is proven, where the functions $\alpha(\varrho)$ and $\chi(S)$ satisfy

(i) $\chi > 0$ and

(ii) $\alpha(0) > 0$, there exists a $\bar{\varrho} > 0$ such that $\alpha(\bar{\varrho}) = 0$
       and $\alpha(\varrho) > 0$ for $0 < \varrho < \bar{\varrho}$.

In Painter and Hillen [36], the authors derive a chemotaxis model comprising a chemotactic sensitivity of this form from a master-equation describing a random walk on a one-dimensional lattice by taking into account the finite size of cells.

Another approach to modeling chemotaxis comes from kinetic theory. There, the phase space density $f(t, x, v)$ of cells at position $x \in \mathbb{R}^n$, moving with velocity $v \in V \subseteq \mathbb{R}^n$ at time $t \geq 0$ is represented by a (linear) kinetic transport equation:

$$f_t + v \cdot \nabla_x f = \int_V [T(v', v)f' - T(v, v')f]dv' := Q(f), \qquad (1.3)$$

with $f' := f(t, x, v')$. The turning kernel $T(v, v')$ describes reorientation of cells, i.e. velocity changes from v to v' and may depend on the chemoattractant concentration S or on its derivatives. The integral $\int T(v, v')dv' := \lambda(v)$ describes the rate at which particles choose a new velocity.

An advantage of kinetic over macroscopic models is that information about the individual behaviour of cells can be directly incorporated into the turning kernel. Transport models have first been applied to chemotaxis by Stroock [51], Alt [2] and Othmer *et al.* [33]. Stroock derived a model describing the motion of flagellated bacteria, which consists of straight forward movement with almost constant speed intercepted by short stops, where a new direction

of movement is chosen (*run and tumble*). Soll and Wessels [50] showed how these movement rules can also be applied to the behaviour of slime molds.

In spite of the different approach, diffusion based models and kinetic equations are closely related. How to obtain a drift-diffusion equation as macroscopic limit of a kinetic model has been investigated by several authors, for instance Patlak [40] or Alt [2]. For a detailed discussion of approaches to this problem see [34]. This macroscopic limit procedure allows to relate information about the movement pattern of individual cells from the kinetic model to macroscopic quantities such as the chemotactic velocity. In Hillen and Othmer [20] and [34], the diffusion limit of (1.3) with and without external bias is studied. Using a parabolic scaling, the authors show that the classical KS-equation can be obtained in the limit for a given smooth chemoattractant concentration. A rigorous proof for the case of a nonlinear coupling to an equation for the chemical is given in Chalub *et al.* [7].

Finally, we also want to mention hyperbolic models for chemotaxis consisting of a system of a cell conservation equation and a momentum balance equation. These can also be derived from kinetic transport equations. In Hillen [19], Cattaneo systems are obtained from a kinetic equation via a moment closure method. Originally derived in 1948 to describe heat transport with finite speed [5], the Cattaneo model is based on the assumption that the flux adapts with a certain rate to changes in the density. In Dolak and Hillen [9], such a model is used to describe aggregation of amoebae and bacteria. In Filbet *et al.* [10], a macroscopic limit is used to derive a mass-momentum system modelling angiogenesis from kinetic equations. In particular, the authors assume that the leading order turning operator preserves momentum.

In order to illustrate the relation between the different classes of models and scalings described above, we regard the special case of (1.3) in one space dimension, with constant particle speed s, i.e. with discrete velocities $v \in \{\pm s\}$. We assume that the turning kernel is given by $T(s, -s) = \mu^+$, $T(-s, s) = \mu^-$, which means that particles moving to the right turn to the left with constant rate μ^+, and left moving particles turn to the right with rate μ^-.

If we write $f(t, x, \pm s) = u^\pm(t, x)$ for the density of right/left moving particles, we obtain the equations

$$
\begin{aligned}
u_t^+ + s u_x^+ &= \mu^- u^- - \mu^+ u^+, \\
u_t^- - s u_x^- &= \mu^+ u^+ - \mu^- u^-.
\end{aligned}
\tag{1.4}
$$

This is the Goldstein-Kac model for a correlated random walk on the real line [14], [26].

For the special case $\mu^+ = \mu^- = \mu$, we can immediately write down a Cattaneo system for the macroscopic density $\varrho = u^+ + u^-$ and the population

flux $j = s(u^+ - u^-)$ (see for instance Hadeler [15]):

$$\varrho_t + j_x = 0, \tag{1.5}$$

$$j_t + s^2 \varrho_x = -2\mu j. \tag{1.6}$$

For more than one space dimension, such a straightforward derivation of a Cattaneo model from a transport equation is not possible, and moment closure methods must be used (see above).

In order to derive the macroscopic limit of system (1.4), we introduce the following scaling of space and time: $x \to x/\varepsilon$, $t \to t/\varepsilon^\alpha$, with ε assumed to be small and $\alpha \in \mathbb{N}$. System (1.4) then reads

$$\varepsilon^\alpha u_t^+ + \varepsilon s u_x^+ = \mu^- u^- - \mu^+ u^+, \tag{1.7}$$

$$\varepsilon^\alpha u_t^- - \varepsilon s u_x^- = \mu^+ u^+ - \mu^- u^-.$$

As a next step, we carry out a Hilbert expansion of the densities $u^\pm$,

$$u^\pm(x,t) = u_0^\pm(x,t) + \varepsilon u_1^\pm(x,t) + \mathcal{O}(\varepsilon^2). \tag{1.8}$$

Using (1.8) in (1.7), we obtain in the limit $\varepsilon \to 0$

$$\mu^- u_0^- - \mu^+ u_0^+ = 0. \tag{1.9}$$

The vector (μ^-, μ^+) spans the kernel of the linear mapping $\mathcal{L} : \mathbb{R}^2 \to \mathbb{R}$, $\mathcal{L}(a,b) = \mu^- b - \mu^+ a$. Let $F^\pm$ be the normalized equilibrium distribution in velocity space given by

$$F^+ = \frac{\mu^-}{\mu^+ + \mu^-} \quad \text{and} \quad F^- = \frac{\mu^+}{\mu^+ + \mu^-}, \quad \text{with} \quad F^+ + F^- = 1. \tag{1.10}$$

Then, for any function $c(x,t)$ depending only on time and space, the vector $c(x,t)(F^+, F^-)$ is in the kernel of $\mathcal{L}$. Therefore, we can define a macroscopic density $\varrho_0(x,t)$ such that

$$u_0^\pm(x,t) = F^\pm \varrho_0(x,t) \quad \text{and} \quad u_0^+(x,t) + u_0^-(x,t) = \varrho_0(x,t). \tag{1.11}$$

Our aim will now be to derive an equation for this macroscopic density.

We add the two equations in (1.7) and obtain

$$\varepsilon^\alpha \varrho_{0,t} + \varepsilon (\varrho_0 j_F)_x = \mathcal{O}(\varepsilon^2), \tag{1.12}$$

where j_F is the flow produced by the equilibrium distribution $F^\pm$,

$$j_F := sF^+ - sF^- = s\frac{\mu^- - \mu^+}{\mu^+ + \mu^-}. \tag{1.13}$$

If $j_F \neq 0$, it can be immediately seen that setting $\alpha = 1$ is an appropriate choice for our macroscopic scaling. This scaling is often called *hydrodynamic* or *hyperbolic scaling*. Dividing (1.12) by ε and letting $\varepsilon \to 0$ yields a conservation equation for the macroscopic density $\varrho_0(x,t)$:

$$\varrho_{0,t} + (\varrho_0 j_F)_x = 0. \tag{1.14}$$

In the case of $\mu^+ = \mu^- := \mu$ however, the mean velocity of the equilibrium distribution is zero, and the above scaling would only give $\varrho_{0,t} = 0$. Hence, we must choose a scaling yielding more information about the ongoing processes and set $\alpha = 2$. This type of scaling is called *diffusive* or *parabolic scaling*. To derive an equation for the macroscopic density, we employ the expansion (1.8) in (1.7) with $\alpha = 2$ and compare orders of ε. From the $\mathcal{O}(1)$ terms, we already deduced equation (1.9). Comparing coefficients of the $\mathcal{O}(\varepsilon)$ terms gives

$$su^+_{0,x} = \mu(u^-_1 - u^+_1), \tag{1.15}$$

$$-su^-_{0,x} = \mu(u^+_1 - u^-_1), \tag{1.16}$$

and hence,

$$u^-_1 - u^+_1 = \frac{s}{2\mu}\varrho_{0,x}. \tag{1.17}$$

Comparing the $\mathcal{O}(\varepsilon^2)$ terms yields

$$u^+_{0,t} + su^+_{1,x} = \mu(u^-_2 - u^+_2), \tag{1.18}$$

$$u^-_{0,t} - su^-_{1,x} = \mu(u^+_2 - u^-_2). \tag{1.19}$$

We add these equations and use (1.17) to obtain the diffusion equation

$$\varrho_{0,t} = \frac{s^2}{2\mu}\varrho_{0,xx}. \tag{1.20}$$

Hence, depending whether the mean velocity of the equilibrium distribution is zero or not, either the diffusion equation (1.20) or the convection equation (1.14) are the corresponding macroscopic equations.

Going back to the convection equation (1.14), we will now derive a diffusion term as an higher order correction, which will regularize the solution. For this purpose, we use an approach known as Chapman-Enskog expansion (see for instance Cercignani [6]). In contrast to the Hilbert expansion (1.8), $u^\pm$ is not expanded into a power series of ε. Instead, the equations themselves are expanded, and the macroscopic density ϱ can actually depend on ε in a complex way. We decompose $u^\pm$ in this form:

$$u^\pm(x,t) = F^\pm \varrho(x,t) + \varepsilon u^\pm_{\mathrm{I}}(x,t), \tag{1.21}$$

where we assume that

$$u^+(x,t) + u^-(x,t) = \varrho(x,t), \tag{1.22}$$

which implies

$$u_\perp^+(x,t) + u_\perp^-(x,t) = 0. \tag{1.23}$$

We introduce $\kappa(x,t) = u_\perp^+(x,t)$ and obtain

$$u^\pm(x,t) = F^\pm \varrho(x,t) \pm \varepsilon\kappa(x,t). \tag{1.24}$$

Using this ansatz in system (1.7) with $\alpha = 1$ yields

$$\varepsilon\big(F^+\varrho_t + sF^+\varrho_x\big) + \varepsilon^2(\kappa_t + s\kappa_x) = -\varepsilon(\mu^+ + \mu^-)\kappa, \tag{1.25}$$

$$\varepsilon\big(F^-\varrho_t - sF^-\varrho_x\big) + \varepsilon^2(-\kappa_t + s\kappa_x) = \varepsilon(\mu^+ + \mu^-)\kappa. \tag{1.26}$$

As we add the equations (1.25) and (1.26) and divide by ε, we obtain

$$\varrho_t + (\varrho j_F)_x + 2\varepsilon s\kappa_x = 0, \tag{1.27}$$

where u_c is again given by (1.13). The $\mathcal{O}(1)$ terms yield again the convection equation (1.14). For the higher order term, we need to express κ in terms of ϱ. To this end we use (1.27) in (1.25) and (1.26) and conclude

$$s\frac{2\mu^+\mu^-}{(\mu^+ + \mu^-)^2}\varrho_x = -(\mu^+ + \mu^-)\kappa + \mathcal{O}(\varepsilon) \tag{1.28}$$

Hence,

$$\kappa = -\frac{2s\mu^+\mu^-}{(\mu^+ + \mu^-)^3}\varrho_x + \mathcal{O}(\varepsilon). \tag{1.29}$$

We use this correction term in (1.27) and neglect quadratic orders of ε to find a drift equation with diffusion correction

$$\varrho_t + (\varrho j_F)_x = \varepsilon\frac{4s^2\mu^+\mu^-}{(\mu^+ + \mu^-)^3}\varrho_{xx}. \tag{1.30}$$

The solution of this equation $\varrho(x,t)$ depends on $\varepsilon > 0$.

We will come across an equation of this type again in the second part of this thesis; in the first part, we will be concerned with kinetic transport models. For biological applications, mostly cases where the mean velocity of the equilibrium distribution vanishes have been treated in the literature ([20], [34], [7]). This implies that directed movement, for instance towards a chemical gradient, is small compared to the unbiased, random motion of cells. In the next chapter, we will investigate the opposite case. Our motivation is the

observed movement pattern of amoeboid cells like *Dictyostelium discoideum* or leukocytes: once the cells respond to the external field, random motion is almost completely suppressed. In a transport model, this is reflected by the fact that the dominating part of the turning kernel depends on the gradient of the chemoattractant. Analogously to the simple, one-dimensional example presented here, the macroscopic limit is based on a hyperbolic scaling in this case and the resulting macroscopic model will be a pure convection equation. Again, we will apply a Chapman-Enskog expansion to derive a diffusion term as higher order correction.

Chapter 2

Kinetic models for chemotaxis

The kinetic models derived in this chapter will be based on the assumption
that the turning behaviour of cells is not only influenced by the chemical con-
centration or its spatial gradient, but also by its temporal variation. Whereas
it is known that flagellated bacteria like *E. coli* are too small to measure
spatial gradients directly and thus decide whether a direction is favourable
or not by sampling information along their cell path, the situation is not so
clear for larger cells such as *Dictyostelium discoideum*. Although they might
be able to measure spatial gradients along their body axis, there is evidence
that they also employ a spatio-temporal mechanism to orient in gradient fields
[55], [56]. It has been experimentally shown that slime mold amoebae alter
their movement pattern according to temporal variations of the chemoattrac-
tant as well as to spatial ones [54], [58]. A recent study demonstrated that
human polymorphonuclear leukocytes respond to spatio-temporal variations
of the chemoattractant fMLP remarkably similar to the way *Dictyostelium*
cells respond to waves of cAMP [13]. Static gradients of chemoattractant in
the body would have to remain steep over large distances for long periods of
time, and although there is no evidence that the signal in the human body
shows temporal variations indeed, it is perceivable that is is a wave-like re-
lay of chemoattractant as found in *Dictyostelium* that attracts leukocytes to
infection sites over large distances.

In the following section, we present a general kinetic model for cell move-
ment incorporating internal degrees of freedom, coupled with an equation for
the chemoattractant. By a moment expansion procedure this model is reduced
to a kinetic equation for the cell distribution on position-velocity space, cou-
pled with transport equations for the average values of the internal degrees of
freedom. A macroscopic scaling of this system is introduced. In section 2.2,
the macroscopic limit of the kinetic equation is discussed. The assumption
that cells have a primitive form of memory leads to a convection equation as a

macroscopic limit, with a chemotactic velocity that depends on the temporal derivative of the chemoattractant. This approximation is justified rigorously for general initial data. Moreover, we formally derive a second order approximation, constructing a regularizing diffusion term by Chapman-Enskog type arguments.

Although the principal ideas and techniques presented here may be applied to describe other forms of eukaryotic chemotaxis, we will use the slime mold *Dictyostelium discoideum* as an example for our model, and perform numerical experiments in section 2.3. Here a model with one internal degree of freedom is used, modelling production and relay of cAMP by a simple activation-inhibition mechanism. Our numerical results show that our modelling approach has the potential to resolve the so-called chemotactic wave paradox.

In section 2.4, we translate formal movement rules for cells as proposed by Dallon and Othmer in [8] to a kinetic equation. In the macroscopic limit, the evolution of cell density is again described by a convection equation, where the flux depends on the temporal variation of the signal concentration.

Finally, we conclude this chapter (section 2.5) by putting it into the context of other attempts for the resolution of the chemotactic wave paradox.

2.1   Kinetic models with internal degrees of freedom

Let $p(t, x, v, \zeta)$ be the phase space density of cells, depending on time t, position $x \in \mathbb{R}^n$, velocity $v \in V$ and an internal variable $\zeta \in Z \subseteq R^k$. The components of ζ are for instance concentrations of chemicals inside the cell. We assume that inside an individual cell, this variable evolves according to

$$\dot{\zeta} = \eta(\zeta, S(t, x(t))), \tag{2.1}$$

where $S(t, x)$ is the outer concentration of the chemoattractant and $x(t)$ is the cell path. Then the evolution of $p(t, x, v, \zeta)$ is governed by the equation

$$p_t + v \cdot \nabla_x p + \nabla_\zeta \cdot (\eta p) = \int_V [T(v', v)p' - T(v, v')p] \, dv' := Q(p). \tag{2.2}$$

We assume that the cell movement is not affected by the internal quantities, whence $T(v, v')$ is independent from ζ. In the following, we will be interested in the position-velocity and, respectively, position densities of cells

$$f(t, x, v) = \int_Z p(t, x, v, \zeta) \, d\zeta, \qquad \varrho(t, x) = \int_V f(t, x, v) \, dv, \tag{2.3}$$

and in the average values $z(t, x)$ of the internal variables

$$(\varrho z)(t, x) = \int_V \int_Z \zeta\, p(t, x, v, \zeta)\, d\zeta dv. \tag{2.4}$$

Integrating (2.2) with respect to ζ gives

$$f_t + v \cdot \nabla_x f = Q(f), \tag{2.5}$$

where we used the boundary condition $p(t, x, v, \zeta) = 0$ for $\zeta \in \partial Z$. On the other hand, multiplication of (2.2) by ζ and integration with respect to ζ and v yields

$$(\varrho z)_t + \nabla_x \cdot \int_V \int_Z \zeta v p\, d\zeta\, dv = \int_V \int_Z \eta p\, d\zeta\, dv. \tag{2.6}$$

In order to be able to write the equations (2.5), (2.6) in a self consistent form, we need closure assumptions for the two integrals. The first one we approximate by

$$\int_V \int_Z \zeta v p\, d\zeta\, dv \approx z \int_V v f dv. \tag{2.7}$$

This condition is, for instance, fulfilled for distribution functions of the form

$$p(t, x, v, \zeta) = f(t, x, v) p_1(t, x, \zeta),$$

which means that the variables v and ζ are uncorrelated. This is compatible with our above assumption that the internal variables ζ have no influence on cell movement. The second closure relation

$$\int_V \int_Z \eta p\, d\zeta\, dv \approx \varrho \hat{\eta}(z, S) \tag{2.8}$$

will depend on the form of η.

For the chemoattractant $S(t, x)$ we choose

$$S_t = D_S \Delta S + \nu(S, z, \varrho), \tag{2.9}$$

the function $\nu(S, z, \varrho)$ describing production and degradation of the chemical in dependence on the cell density and the inner state of the cells.

We non-dimensionalize the equations (2.5), (2.6) and (2.9) by choosing a reference time t_0, length x_0 and speed v_0. Dimensionless quantities are introduced according to

$$x = x_0 \bar{x}, \quad t = t_0 \bar{t}, \quad v = v_0 \bar{v},$$

$$T(v, v') = T_0 \bar{T}\left(\frac{v}{v_0}, \frac{v'}{v_0}\right), \quad f(x, v, t) = f_0 \bar{f}\left(\frac{t}{t_0}, \frac{x}{x_0}, \frac{v}{v_0}\right).$$

T_0 is a typical value for the size of the turning kernel, and v_0 is a typical speed for velocities in V assumed bounded (since cells can only move with some maximal speed). We fix the length scale such that $x_0 = v_0 t_0$. The quantity $T_0 v_0^3$ can be interpreted as turning rate, i.e. the inverse of the mean free run time $\tau_f = T_0^{-1} v_0^{-3}$. Furthermore, we choose

$$\hat{\eta}(z,S) = \frac{z_0}{t_0} \bar{\hat{\eta}}_0 \left(\frac{z}{z_0}, \frac{S}{S_0} \right), \quad \nu(S, \varrho, z) = \frac{S_0}{t_0} \bar{\nu} \left(\frac{S}{S_0}, \frac{\varrho}{\varrho_0}, \frac{z}{z_0} \right)$$

$$S(t,x) = S_0 \overline{S} \left(\frac{t}{t_0}, \frac{x}{x_0} \right), \quad z(t,x) = z_0 \bar{z} \left(\frac{t}{t_0}, \frac{x}{x_0} \right), \quad \varrho(t,x) = \varrho_0 \bar{\varrho} \left(\frac{t}{t_0}, \frac{x}{x_0} \right).$$

We fix the length scale by setting $\frac{x_0^2}{t_0} = D_S$. Dropping the bars, the scaled version of (2.5), (2.6), (2.9) reads

$$\varepsilon f_t + \varepsilon v \cdot \nabla_x f = \int_V \left[T(v', v) f' - T(v, v') f \right] dv' \quad (2.10)$$

$$(\varrho z)_t + \nabla_x \cdot \left(z \int_V v f \, dv \right) = \varrho \hat{\eta}(z, S) \quad (2.11)$$

$$S_t = \Delta S + \nu(S, z, \varrho). \quad (2.12)$$

Our main scaling assumption is that the dimensionless parameter

$$\varepsilon = \frac{\tau_f}{t_0} = \frac{v_0^2 \tau_f}{D_S}$$

is small. Also we assume that the scaled functions $\hat{\eta}$ and ν are of moderate size.

2.2 Cell movement - macroscopic limit

We assume that cells have a form of short memory, allowing them to compare present chemical concentrations to previous ones and thus to respond to temporal gradients along their paths. The decision whether to change direction and turn or to continue moving is then based on the concentration profile of the chemical S a cell experiences. In the limit of an infinitesimal short time interval for the sampling of information, this means dependence on the directional derivative $S_t + v \cdot \nabla S$. Note that this is the correct scaled form of the directional derivative, due to the hydrodynamic scaling assumption $x_0 = v_0 t_0$ (as opposed to the diffusion scaling $x_0 \sqrt{\varepsilon} = v_0 t_0$) guaranteeing that the terms S_t and $v \cdot \nabla S$ are of equal importance. We assume that $T(v, v')$ is of the form

$$T(v, v') = \varphi(S_t + v \cdot \nabla S), \quad (2.13)$$

with $\varphi(S_t + v \cdot \nabla S)$ being a monotonically decreasing function. Evolution of the cell density is therefore described by (2.10) with

$$Q(f) = \int_V [\varphi(S_t + v' \cdot \nabla S)f' - \varphi(S_t + v \cdot \nabla S)f] dv'. \qquad (2.14)$$

We investigate the limit $\varepsilon \to 0$ in (2.10), with the turning operator given by (2.14), and subject to initial conditions

$$f(t = 0) = f_I. \qquad (2.15)$$

For the data, we make the following assumptions:

Assumption 1
The turning kernel $\varphi : \mathbb{R} \to \mathbb{R}$ is smooth, monotonically decreasing, and satisfies

$$0 < \gamma \le \varphi \le \Gamma.$$

Assumption 2
The functions $S(t, x)$ and $f_I(x, v)$ are smooth. Besides, $f_I(x, v) = 0$ for $x \notin K$, K compact. The set of velocities V is bounded and rotationally symmetric.

Lemma 1
Let the assumption 1 hold. Then, for given $S_t \in \mathbb{R}$ and $\nabla S \in \mathbb{R}^n$, the kernel of the turning operator $Q(f)$ given by (2.14) is one-dimensional and spanned by the equilibrium distribution

$$F(v) = \frac{1}{A\varphi(S_t + v \cdot \nabla S)}, \quad A = \int_V \frac{dv'}{\varphi(S_t + v' \cdot \nabla S)}$$

satisfying $F(v) > 0$ and $\int_V F(v)dv = 1$. For $g \in L^2(V; dv/F)$, the equation $Q(f) = g$ has a unique solution $f \in L^2(V; dv/F)$ satisfying $\int_V f\,dv = 0$, iff $\int_V g\,dv = 0$.

Proof. It can be easily checked that the turning operator Q is symmetric on the space $L^2(V; dv/F)$. Then the Fredholm alternative states that there exists a solution $f = Q^{-1}(g)$ if and only if g is orthogonal to the kernel of Q in the space $L^2(V; dv/F)$. Requiring $\int_V f\,dv = 0$ determines the solution uniquely. The solution f can also be calculated explicitly, i.e. $f = \frac{(c-g)}{\varphi|V|}$. This solves the equation $Q(f) = g$ for every constant $c = \int_V \varphi f dv$, provided that g satisfies the solvability condition. The condition $\int_V f\,dv = 0$ then uniquely determines the constant, $c = \int_V gF dv$. $\square$

We want to admit general initial conditions f_I, which means that $Q(f_I) = 0$ cannot be assumed to hold. This leads to an initial layer. Introducing a fast time scale $\tau = \frac{t}{\varepsilon}$, we make the two scale ansatz

$$f(t, x, v) = \bar{f}(t, x, v) + \hat{f}(\tau, x, v),$$ (2.16)

where $\bar{f}$ is the outer solution and $\hat{f}$ a layer correction satisfying $\hat{f}(\infty, x, v) = 0$. Both $\hat{f}$ and $\bar{f}$ solve the (linear, homogeneous) transport equation (2.10), and they are only coupled via the initial conditions $\bar{f}(t = 0) + \hat{f}(\tau = 0) = f_I$. For both contributions, we shall construct asymptotic expansions: $\bar{f} = \bar{f}_0 + \varepsilon \bar{f}_1 + O(\varepsilon^2)$ and $\hat{f} = \hat{f}_0 + \varepsilon \hat{f}_1 + O(\varepsilon^2)$, satisfying the initial conditions:

$$\bar{f}_0(t = 0) + \hat{f}_0(\tau = 0) = f_I,$$ (2.17)

$$\bar{f}_1(t = 0) + \hat{f}_1(\tau = 0) = 0.$$ (2.18)

Inserting the expansion for the outer solution into (2.10), we obtain

$$Q(\bar{f}_0) = 0$$ (2.19)

$$\frac{\partial \bar{f}_0}{\partial t} + v \cdot \nabla_x \bar{f}_0 = Q(\bar{f}_1).$$ (2.20)

From the first equation, we get that $\bar{f}_0(t, x, v) = \varrho_0(t, x) F(v; t, x)$ where F depends on (t, x) through $S_t(t, x)$ and $\nabla S(t, x)$. The solvability condition for (2.20) implies that the evolution of the macroscopic cell density ϱ_0 is given by

$$\frac{\partial \varrho_0}{\partial t} + \nabla \cdot (\varrho_0 u_c) = 0, \quad u_c = \int_V v F \, dv.$$ (2.21)

By the rotational symmetry of V, the macroscopic chemotactic velocity u_c is proportional to ∇S:

$$u_c = \chi(S_t, |\nabla S|) \nabla S, \quad \chi(S_t, |\nabla S|) = \frac{1}{A|\nabla S|} \int_V \frac{v_1 dv}{\varphi(S_t + v_1 |\nabla S|)}.$$ (2.22)

The non-negativity of the chemotactic sensitivity χ is a consequence of the assumption that φ is decreasing.

The first order correction is then of the form

$$\bar{f}_1 = Q^{-1}\left(\frac{\partial \bar{f}_0}{\partial t} + v \cdot \nabla \bar{f}_0\right) + \varrho_1 F.$$ (2.23)

For the initial layer correction, we make the dependence of the turning operator on time $t = \varepsilon \tau$ (through S_t and ∇S) visible by the notation $Q(\hat{f}) = Q(\varepsilon \tau)(\hat{f})$ and get

$$\frac{\partial \hat{f}_0}{\partial \tau} = Q(0)(\hat{f}_0)$$ (2.24)

$$\frac{\partial \hat{f}_1}{\partial \tau} + v \cdot \nabla_x \hat{f}_0 = Q(0)(\hat{f}_1) + \tau Q_t(0)(\hat{f}_0),$$ (2.25)

where Q_t denotes the derivative of the operator Q with respect to time. Integration of (2.24) and (2.25) with respect to v gives

$$\frac{\partial}{\partial \tau} \int_V \hat{f}_0 \, dv = 0, \quad \frac{\partial}{\partial \tau} \int_V \hat{f}_1 \, dv + \int_V v \cdot \nabla_x \hat{f}_0 \, dv = 0, \tag{2.26}$$

with the consequence

$$\int_V \hat{f}_0(\tau = 0) dv = 0, \quad \int_V \hat{f}_1(\tau = 0) dv - \int_V \int_0^\infty v \cdot \nabla_x \hat{f}_0 \, d\tau dv = 0. \tag{2.27}$$

Initial conditions for the macroscopic densities ϱ_0 and ϱ_1 are then derived from (2.17), (2.18). Actually, ϱ_1 will be chosen independently of time $(\varrho_1 = \varrho_1(x))$:

$$\varrho_0(t = 0) = \int_V f_I \, dv \tag{2.28}$$

$$\varrho_1 = -\int_V \int_0^\infty v \cdot \nabla_x \hat{f}_0 \, d\tau dv. \tag{2.29}$$

This in turn fixes the initial conditions for the layer corrections:

$$\hat{f}_0(\tau = 0) = f_I - F \int_V f_I \, dv \tag{2.30}$$

$$\hat{f}_1(\tau = 0) = -Q^{-1} \left(\frac{\partial \bar{f}_0}{\partial t} + v \cdot \nabla_x \bar{f}_0 \right)(t = 0) + F \int_V \int_0^\infty v \cdot \nabla_x \hat{f}_0 \, d\tau dv. \tag{2.31}$$

Now the approximate solution is constructed in several steps. First we consider the problem (2.21), (2.28) for ϱ_0. By assumption 2, the macroscopic chemotactic velocity u_c is smooth, and the same holds for the initial datum $\varrho_0(t = 0)$, which also satisfies $\varrho_0(t = 0) \in L^1(\mathbb{R}^n)$. By the method of characteristics, (2.21), (2.28) has a smooth solution $\varrho_0 \in L^\infty((0, \infty), L^1(\mathbb{R}^n))$.

The next step is the construction of $\hat{f}_0$:

Theorem 1

Let the assumptions 1 and 2 hold. Then the problem (2.24),(2.30) has a unique smooth solution $\hat{f}_0$ satisfying

$$\|\hat{f}_0(\tau, \cdot, \cdot)\|_{L^1(\mathbb{R}^n; L^2(V))} \le c e^{-\kappa \tau} \|f_I\|_{L^1(\mathbb{R}^n; L^2(V))}, \quad c, \kappa > 0. \tag{2.32}$$

Proof. With $\varphi_0 = \varphi(t = 0)$ we define the entropy

$$H = \frac{1}{2} \int_V \hat{f}_0^2 \, \varphi_0 \, dv. \tag{2.33}$$

By assumption 1, $\sqrt{H}$ is equivalent to the $L^2(V)$-norm. We have

$$
\begin{aligned}
\frac{dH}{d\tau} &= \int_V Q(0)(\hat{f}_0)\hat{f}_0\,\varphi_0\,dv \\
&= -\frac{1}{2}\iint_V (\hat{f}_0'\varphi_0' - \hat{f}_0\varphi_0)^2 dv'dv \\
&\leq -\frac{\gamma^2}{2}\iint_V \frac{1}{\varphi_0\varphi_0'}(\hat{f}_0'\varphi_0' - \hat{f}_0\varphi_0)^2 dv'dv \\
&= -\gamma^2 \int_V \frac{dv}{\varphi_0}\int_V \hat{f}_0^2\varphi_0\,dv \leq -\frac{2\gamma^2|V|}{\Gamma}H.
\end{aligned}
$$

$\square$

The partial derivative $g_i = \frac{\partial \hat{f}_0}{\partial x_i}$ of $\hat{f}_0$ satisfies the inhomogeneous version

$$
\frac{\partial g_i}{\partial \tau} = Q(0)(g_i) + Q_{x_i}(0)(\hat{f}_0) \tag{2.34}
$$

of (2.24) with an exponentially decaying inhomogeneity. Exponential decay of g_i and then also of the solution $\hat{f}_1$ of (2.25), (2.31) is proven similarly to the proof above. Finally, ϱ_1 is computed from (2.29) completing the construction of the approximate solution.

Theorem 2
Let the assumptions 1 and 2 hold and let $T > 0$. Let f, $\hat{f}_0$ and ϱ_0 be the solutions of the problems (2.10), (2.15); (2.24), (2.30) and, respectively, (2.21), (2.28) for $t < T$. Then there exists a positive constant C_T which depends on the data such that

$$
\sup_{0<t<T}\|f(t,\cdot,\cdot) - \varrho_0(t,\cdot)F(\cdot;t,\cdot) - \hat{f}_0(\frac{t}{\varepsilon},\cdot,\cdot)\|_{L^1(\mathbb{R}^n\times V)} \leq C_T\varepsilon.
$$

Proof. The proof is based on an estimate of the remainder $r = f - (\bar{f}_0 + \varepsilon\bar{f}_1) - (\hat{f}_0 + \varepsilon\hat{f}_1)$ solving a problem of the form (2.10), (2.15) with vanishing initial data and an $O(\varepsilon^2)$-inhomogeneity in the transport equation. The estimation of r is as in [42], where a problem without initial layer has been considered. $\square$

The above procedure for computing approximations of the outer solution is the Hilbert expansion. An alternative approach is the Chapman Enskog expansion which is based on the decomposition

$$
f(t,x,v) = \varrho(t,x)F(t,x;v) + \varepsilon f^\perp(t,x;v), \tag{2.35}
$$

$$
\varrho = \int_V f\,dv \tag{2.36}
$$

of the distribution function. The basic idea is to find approximations of the equation for ϱ (derived by applying the projection (2.36) to the kinetic equation (2.10)):

$$\varrho_t + \nabla \cdot \left(\varrho u_c + \varepsilon \int_V v f^\perp dv \right) = 0. \tag{2.37}$$

To determine the $\mathcal{O}(\varepsilon)$ correction term in (2.37), we have to compute $f^\perp$. Equation (2.10) yields

$$Q(f^\perp) = v \cdot \nabla(F\varrho) - F\nabla \cdot (\varrho u_c) + \varrho F_t + \mathcal{O}(\varepsilon). \tag{2.38}$$

Neglecting, the $\mathcal{O}(\varepsilon)$ term, we can compute the lowest order approximation to $f^\perp$ explicitly:

$$f_0^\perp = h_1 \cdot \nabla \varrho + \varrho h_2 \tag{2.39}$$

with

$$Q(h_1) = F(v - u_c), \quad Q(h_2) = v \cdot \nabla F - F\nabla \cdot u_c + F_t,$$

and

$$\int_V h_i \, dv = 0.$$

Inserting this into (2.37) yields the drift-diffusion equation

$$\varrho_t + \nabla \cdot \left(\varrho(u_c + \varepsilon u_1) - \varepsilon D\nabla \varrho \right) = 0, \tag{2.40}$$

where the diffusion tensor D and the correction to the chemotactic velocity are given by

$$D = -\int_V v \otimes h_1 \, dv, \quad u_1 = -\int_V v \, h_2 \, dv \tag{2.41}$$

Lemma 2
The tensor D is symmetric and positive definite.

Proof. We write the diffusion tensor D as

$$D = -\int_V (v - u_c) \otimes h_1 \, dv = -\int_V \frac{Q(h_1) \otimes h_1}{F} dv.$$

Using the entropy equality

$$\int_V \frac{Q(f)g}{F} dv = -\frac{1}{2A} \int_V \int_V \left(\frac{f}{F} - \frac{f'}{F'} \right) \left(\frac{g}{F} - \frac{g'}{F'} \right) dv dv', \tag{2.42}$$

the symmetry of D immediately follows and we can estimate the quadratic form $z^{tr} D z$ by

$$z^{tr} D z = -\int_V \frac{Q(z \cdot h_1) z \cdot h_1}{F} dv \geq 0. \tag{2.43}$$

The equality sign only applies in the case when $z \cdot h_1$ is an equilibrium distribution, i.e. $Q(z \cdot h_1) = F(v - u_c) \cdot z = 0$ for all $v \in V$. As long as the velocity space V consists of more than one velocity vector, this never happens, and D is positive definite.   □

The rotational symmetry of the problem is broken because there is one distinguished direction, namely the direction of the chemical gradient. Thus, the tensor D is in general anisotropic and $D = P\widehat{D}P^{-1}$, with

$$\widehat{D} = \begin{pmatrix} d_1 & 0 \\ 0 & d_2 I_{n-1} \end{pmatrix} \tag{2.44}$$

and P is an orthogonal matrix whose first column is $\frac{\nabla S}{|\nabla S|}$. If $\nabla S = 0$, D is isotropic, i.e. $d_1 = d_2$.

2.3   Application to *Dictyostelium discoideum*

When starving, the slime mold amoeba *Dictyostelium discoideum* migrates towards the source of waves of the chemoattractant cAMP (see Introduction). This peculiar behaviour gives rise to the so-called chemotactic wave paradox: If the chemotactic response of cells was only determined by the gradient of the chemoattractant, cells would move in direction of the source in the wave front (positive spatial gradient), but change direction and follow the wave once they are in the wave back (negative spatial gradient). Little or no aggregation of cells should be expected. This is clearly not what happens: it is known that cells move in the wave front, but remain more or less stationary in the wave back [49], see Fig. 2.1.

Experiments where Dd cells were stimulated with shifting, spatially homogeneous concentrations of cAMP imitating the temporal dynamics of a natural wave showed that in the increasing phase, turning is suppressed and cells move in a directionally persistent way, whereas translocation of cells is dramatically reduced when the concentration is decreasing (see e.g. [58]). In contrast to this, experiments showed that constant concentrations of cAMP are not able to stimulate motility, and that high concentrations actually suppress cell movement.

In the following, we focus on the early stages of the cell cycle, i.e. the formation of aggregates. We present a kinetic model where the turning kernel describes qualitatively the cell behaviour described above, and solve the corresponding macroscopic model numerically.
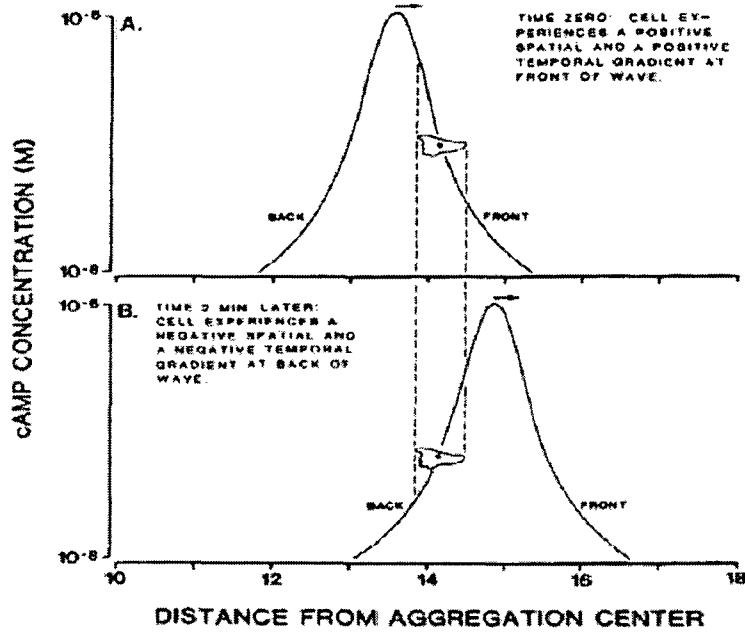
Figure 2.1: The chemotactic wave paradox [49]

2.3.1   Model equations

Since we are mainly concerned with modeling cell movement and also in view of the numerical experiments we will carry out later, we confine ourselves to using a very simple model for cAMP production. It is in fact a further simplification of a toy model proposed by Othmer and Schaap [35]. Although this model has no concrete biochemical background, it captures the essential features of the system. In the framework of the general model presented in section 2.1, the function $S(t, x)$ now represents the cAMP concentration. We postulate the existence of an internal chemical with concentration w, which is activated by external cAMP and inhibited by a second internal chemical with concentration ζ:

$$w = (w_0 + h(S) - \zeta)_+ \tag{2.45}$$

with $h(S) = \frac{1}{1+S}$ describing transduction of the internal signal. Our modifications of the toy model from [35] are in this equation. The first one is the replacement of an ODE for w by the quasi-steady approximation (2.45). The second is the cutoff by taking the positive part, allowing to interpret w an a chemical concentration. The dynamics of the second chemical aims at

restoring the equilibrium value w_0 of w (adaption):

$$\dot{\zeta} = \eta(\zeta, S) = \frac{1}{\tau_z}(h(S) - \zeta). \tag{2.46}$$

Finally, we assume that the production of external cAMP by the cell is triggered by the first chemical:

$$\dot{S} = \varrho w - g(S), \tag{2.47}$$

where $g(S) = \frac{1}{\tau_S}S(1 + \frac{S}{S_1})$ models degradation of S. The saturation of $h(S)$ as $S \to \infty$ and the quadratic term in $g(S)$ both stabilize the system. One of these two assumptions would be sufficient for this purpose, but we keep them both. After elimination of w by (2.45), one internal variable $\zeta \in Z = [0, \infty)$ remains. By the linearity of $\eta(\zeta, S)$ with respect to ζ, the moment closure relation (2.8) is an equality with $\hat{\eta} = \eta$. The above equations are in dimensionless form. The reference values z_0, S_0, ϱ_0 (unspecified in section 2.1) have been chosen such that the number of parameters is reduced.

Our final Dd model is a macroscopic approximation of (2.10)-(2.12):

$$\varrho_t + \nabla \cdot J = 0 \tag{2.48}$$

$$(\varrho z)_t + \nabla \cdot (Jz) = \varrho \frac{h(S) - z}{\tau_z} \tag{2.49}$$

$$S_t = \Delta S + \left[h(S) - z + w_0\right]_+ \varrho - g(S) \tag{2.50}$$

with

$$h(S) = \frac{S}{1 + S} \quad \text{and} \quad g(S) = \frac{1}{\tau_S}S\left(1 + \frac{S}{S_1}\right). \tag{2.51}$$

As a simplification of the macroscopic cell flux in (2.40) derived by the Chapman Enskog expansion, we restrict to a constant, isotropic diffusivity D and neglect the correction εu_1 to the chemotactic velocity. Thus, the cell flux J is given by

$$J = \varrho \chi(S_t, |\nabla S|)\nabla S - \varepsilon D \nabla \varrho. \tag{2.52}$$

In correspondence to a typical experimental setup (cells in petri dishes), we consider a two dimensional position domain $\Omega \subset \mathbb{R}^2$. Along the boundary of Ω, we impose zero flux conditions:

$$\nabla S \cdot \nu = J \cdot \nu = 0 \quad \text{on } \partial\Omega, \tag{2.53}$$

with the normal vector ν. An initial-boundary value problem is completed by prescribing initial data for ϱ, z and S.

2.3.2 Dynamics of the chemoattractant

To begin with, we neglect cell movement and chemoattractant diffusion and investigate spatially homogeneous solutions of (2.48) - (2.50) with $J = 0$:

$$z_t = \frac{h(S) - z}{\tau_z}, \tag{2.54}$$

$$S_t = \left[h(S) - z + w_0\right]_+ \varrho - g(S). \tag{2.55}$$

Depending on the choice of parameters, the system displays the important properties of the signal production and relay mechanism of Dd.

For $w_0 > 0$, the steady state (z_∞, S_∞), uniquely defined by $g(S_\infty) = \varrho w_0$, $z_\infty = h(S_\infty)$, is unstable iff $\varrho h'(S_\infty) - g'(S_\infty) - \frac{1}{\tau_z} > 0$, which we assume in the following. By the simple observations

$$
\begin{aligned}
z_t &\geq 0 \quad \text{for} \quad z = 0, \\
z_t &\leq 0 \quad \text{for} \quad z \geq h(S), \\
S_t &\geq 0 \quad \text{for} \quad S = 0, \\
S_t &\leq \left[h(S) + w_0\right]_+ \varrho - g(S) \leq 0 \quad \text{for } S \text{ large enough,}
\end{aligned}
\tag{2.56}
$$

rectangles of the form $[0, h(\bar{S})] \times [0, \bar{S}]$ in the (S, z)-plane contain the unstable steady state (S_∞, z_∞) and are positively invariant for (2.54), (2.55), if $\bar{S}$ is chosen large enough. Consequently, a stable periodic limit cycle exists by the Poincaré-Bendixon theorem (see the phase portrait, Fig. 2.2). For small values of w_0, the steady state is close to the origin and the limit cycle takes the form of pulses whose separation in time can be regulated by the choice of w_0 (Fig. 2.3 left). This corresponds to the way pacemaker cells secrete the chemical in a periodic fashion. With the same set of parameters, but without constant production of cAMP (i.e., $w_0 = 0$), a non-zero initial condition for S elicits only one single pulse of cAMP, as can be observed in ordinary, relay-competent cells (Fig. 2.3 right).

For further numerical experiments, we will hence assume that there are two different types of cell densities: ordinary cells that do not produce cAMP without external stimulation and "pacemaker" cells with a nonzero rate of constant production. Both cell types contribute to the cAMP dynamics, and both respond to chemical gradients. Consequently, we also have to calculate the values of the internal variable z separately for pacemakers and ordinary cells. We put small discs of pacemaker cells inside the domain, surrounded by ordinary, relay-competent cells. Still neglecting cell movement, we solve the equations (2.49) and (2.50) with $J = 0$, $\varrho = const.$ numerically in a rectangular domain using an operator splitting scheme: first, the reaction terms are solved semi-implicitly, then the diffusion term in (2.50) is integrated using a standard
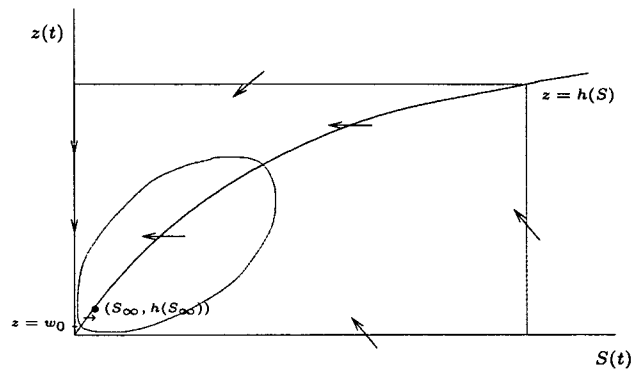
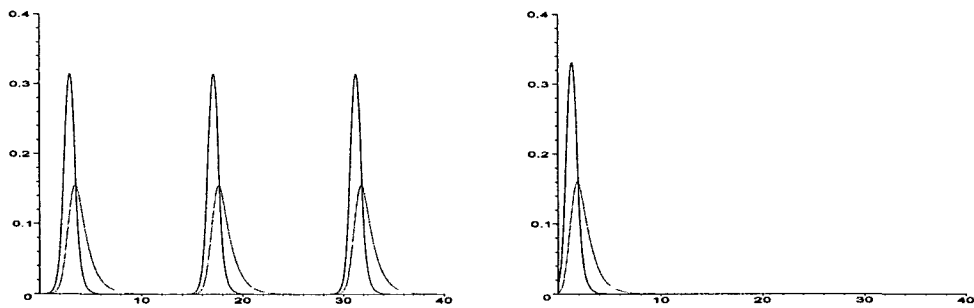Figure 2.2: Phaseportrait for S and z

Figure 2.3: Concentration of S (dark) and z (light) as a function of time. Parameter values: $S_0 = 1.4$, $\tau_S = 0.4$, $\tau_z = 1.0$, $w_0 = 10^{-5}$ (left), $w_0 = 0.0$ (right)
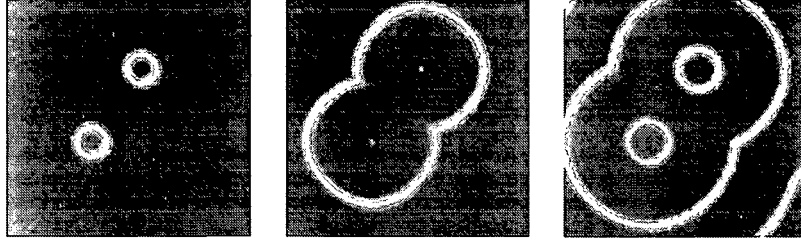
Figure 2.4: Time sequence of cAMP waves on a square domain. Parameter values: $S_1 = 1.4$, $\tau_S = 0.4$, $\tau_z = 1.0$, $w_0 = 0$ for ordinary cells. For pacemaker cells, $w_0 = 10^{-5}$.

ADI-method, which allows us to take larger time steps. Fig. 2.4 shows the time evolution of the cAMP concentration. Pacemaker cells are located at two different sites. From there, wavefronts are initiated and spread over the lawn of relay-competent cells.

2.3.3 Cell Aggregation

Before we can test the full macroscopic model numerically, we have to specify the turning kernel of the kinetic model and calculate the chemotactic velocity according to (2.22). In the following, we will assume that cells move with constant (scaled) speed 1. The velocity space is then given by $V = \{v \in \mathbb{R}^2 : |v| = 1\}$. So far, we have not made any restrictions on $\varphi(S_t + v \cdot \nabla S)$ other than that it has to be a bounded, positive and decreasing function. In the limit of vanishing ∇S, the chemotactic sensitivity is given by

$$\chi(S_t, 0) = -\frac{\varphi'(S_t)}{\mu(V)\varphi(S_t)} \int_V v_1^2 dv. \tag{2.57}$$

¿From the behaviour of cells moving towards a natural source of cAMP, we know that this expression has to grow in S_t. This gives another condition on the turning kernel φ, namely that $-\frac{\varphi'}{\varphi}$ has to be an increasing function.

In Rivero et al. [46], a one-dimensional model for bacterial chemotaxis is proposed. There, the probability per unit time for a cell changing its direction from right-going to left-going and vice versa is proportional to $\exp(-\frac{c_0}{(c_1+S)^2}(S_t \pm vS_x))$, respectively, with c_0 and c_1 constant. It can be derived by assuming that the logarithm of the mean run time of bacteria is proportional to the rate of change of the receptors binding the chemoattractant. If we take up that idea and assume that for two space dimensions, $\varphi(S_t + v \cdot \nabla S) = \exp(-\frac{c_0}{(c_1+S)^2}(S_t + v \cdot \nabla S))$, we see that in this case, $-\frac{\varphi'}{\varphi}$ is constant with respect to S_t and that the chemotactic sensitivity $\chi(S_t, 0)$ does not depend on

S_t.

For the numerical simulations presented here, we choose the function

$$\varphi(S_t + v \cdot \nabla S) = 1 - \tanh\left(\frac{S_t + v \cdot \nabla S - \alpha_1}{\alpha_2}\right), \qquad (2.58)$$

with α_1, α_2 constants and $\alpha_2 > 0$. It is crucial for resolving the chemotactic wave paradox that this choice of φ satisfies the requirement that $\frac{\varphi'}{\varphi}$ is increasing. Apart from that it is bounded, i.e., the mean run time between two turning events is bounded from below. Computing the chemotactic velocity u_c according to (2.22), we obtain for the chemotactic sensitivity

$$\chi(S_t, |\nabla S|) = \frac{e^{\frac{2}{\alpha_2}(S_t - \alpha_1)} B_1\left(\frac{2|\nabla S|}{\alpha_2}\right)}{|\nabla S|\left[1 + e^{\frac{2}{\alpha_2}(S_t - \alpha_1)} B_0\left(\frac{2|\nabla S|}{\alpha_2}\right)\right]}, \qquad (2.59)$$

where B_0 and B_1 are the modified Bessel functions of the first kind of order zero and one, respectively. For $\nabla S \to 0$, we have

$$\chi(S_t, 0) = \frac{1}{\alpha_2\left(1 + e^{-\frac{2}{\alpha_2}(S_t - \alpha_1)}\right)}, \qquad (2.60)$$

which is an increasing function of S_t.

We solve the full system (2.48)-(2.52) numerically by using a time-explicit scheme for (2.48) with upwinding for the transport term. The transport of z along with the cells is treated in a straightforward way, the kinetics of z and S are computed like described before. Additionally, we update the chemotactic sensitivity at every time step according to the new concentration of the chemoattractant. Fig. 2.5 shows the evolution of the cell density ϱ. Cells move towards the source of the chemoattractant waves initiated by pacemaker cells located at two sites in the domain. The dependence of the chemotactic sensitivity on the temporal variation of the chemical prevents them to follow the waves and leads to the formation of two distinct cell aggregates.

In fig. 2.6, we compare, for a different set of parameters, the numerical solution of (2.48)-(2.52) with the chemotactic sensitivity according to (2.59) to the case of a constant sensitivity. The centre shows the cell density ϱ after about 20 waves of cAMP (one of which is shown in the left picture) have passed. On the right, the solution for identical parameter values, but a constant chemotactic sensitivity is shown. No significant aggregation effect can be observed. Fig. 2.7 compares the chemotactic sensitivities and the cell fluxes for the wave profile shown on the left in both cases (dark for $\chi = const.$, light for χ given by (2.59)). The chemoattractant wave is moving to the left.
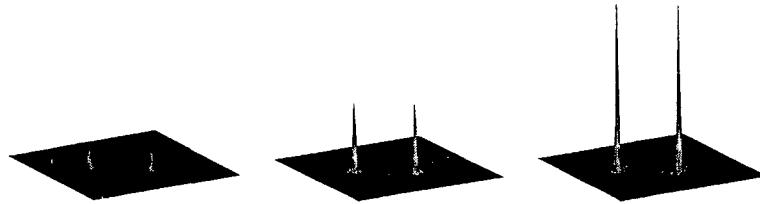
Figure 2.5: Numerical solution of (2.48)-(2.50) with the chemotactic sensitivity given by (2.59) at three different time levels. Parameter values for chemical pathway like for fig. 2.4, and additionally $\varepsilon D = 0.05$, $\alpha_1 = 0.9$, $\alpha_2 = 0.2$.

Although the total flux is larger for a constant sensitivity, cells reverse their direction at the back of the wave, whereas the flux in the non-constant case only points into the direction of the aggregation centre. This eventually leads to the formation of a cell aggregate, as shown in fig. 2.6.

2.4 A kinetic model based on formal movement rules

2.4.1 Cell movement

In Dallon and Othmer [8], a discrete cell model for aggregation of Dd is presented. The chemical dynamics are described by the Tang-Othmer model [52], [53], consisting of four ordinary differential equations for chemical concentrations inside the cells and a diffusion-reaction equation for the outer cAMP-concentration. The movement of cells is determined by formal rules. We want to translate their movement rules into a transport equation. Two sets of rules are discussed. The first one reads:

1. A cell moves if the temporal derivative of the extracellular cAMP concentration is above a certain threshold.

2. All cells move for a fixed duration in the direction of the cAMP gradient at the cell when the motion was started.

3. The cells move with a fixed speed, s_0.

In a second set of rules, the fixed duration of movement has been abandoned and the cells move only if the concentration of one of the internal chemicals is above a threshold. The authors do not incorporate random migration or diffusion into their model, arguing that this component is suppressed when the cells receive a super threshold chemotactic signal.
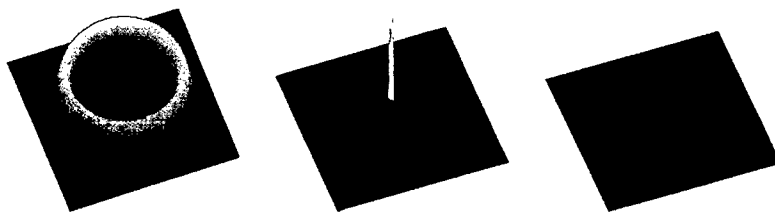
Figure 2.6: Numerical solution of system (2.48)-(2.50) (see text). Parameter values for chemical pathway like in fig. 3.6 and additionally $\varrho_{max} = 30$, $\varepsilon D = 0.005$, $\alpha_1 = 0.2$, $\alpha_2 = 0.9$.
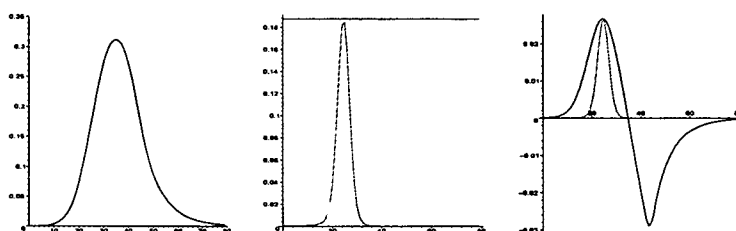

Figure 2.7: Sideview of a cAMP wave traveling to the left, the corresponding chemotactic sensitivities and the cell fluxes in x-direction (light for χ given by (2.59), dark for $\chi = const.$)

To describe these rules by a continuum model, we split the distribution of cells into two parts: the density $r(t, x)$ of resting cells and the distribution density $f(x, v, t)$ of cells moving with velocity $v \in S_0 = \{v : |v| = s_0\}$. We state that the evolution of $f(x, v, t)$ is given by

$$f_t + v \cdot \nabla f = \phi(S_t)\delta(v - v_c)r - \psi(S_t)f := \widetilde{Q}(f, r). \qquad (2.61)$$

The function $\phi(S_t) > 0$ is monotonically increasing: the bigger the temporal derivative of S becomes, the more cells start moving. Assuming that cells can only move with constant speed s_0, we define the microscopic chemotactic velocity v_c by $v_c = s_0 \frac{\nabla S}{|\nabla S|}$. The delta function ensures that cells move only in the direction of the chemical gradient. The function $\psi(S_t) > 0$ is decreasing and makes the cells stop again. The density of resting cells is described by

$$r_t = -\int_{S_0} \widetilde{Q}(f, r)dv = \psi(S_t)\int_{S_0} f dv - \phi(S_t)r, \qquad (2.62)$$

where dv denotes the surface measure along the sphere S_0. In a way, the equations are a combination of the movement rules described above: duration of movement is not fixed, but depends on the temporal variation of S, instead of an arbitrary internal variable. Note that this model can be put in the general form (1.3) with $V = S_0 \cup \{0\}$ and

$$\begin{aligned}
T(v,v') &= 0 & \text{for } v,v' \in S_0, \\
T(v,0) &= \psi(S_t) & \text{for } v \in S_0, \\
T(0,v) &= \phi(S_t)\delta(v - v_c) & \text{for } v \in S_0.
\end{aligned}$$

In contrast to the turning kernel from section 2.2, this kernel does not fulfill the assumption 1.

Scaling the equations like in section 2.1 yields

$$\varepsilon f_t + \varepsilon v \cdot \nabla f = \phi(S_t)\delta(v - v_c)r - \psi(S_t)f \tag{2.63}$$

and

$$\varepsilon r_t = -\int_{S_0} Q(f,r)dv. \tag{2.64}$$

2.4.2 Formal Limit

In this section, we investigate the formal limit $\varepsilon \to 0$ of (2.63) and (2.64). In [18], a similar model, considering also death and birth processes is introduced, and its diffusion limit is investigated.

Here, the macroscopic density $\varrho(t,x)$ is given by

$$\varrho = r + \int_{S_0} f dv. \tag{2.65}$$

In the limit $\varepsilon \to 0$, $Q(f_{eq}, r) = 0$ must hold. Obviously, there is a one-dimensional set of equilibrium distributions, parametrized by r_{eq} and satisfying

$$f_{eq} = \frac{\phi}{\psi}r_{eq}\delta(v - v_c). \tag{2.66}$$

Integrating (2.63) with respect to v, adding (2.64) and dividing by ε yields the convection equation

$$\varrho_t + \nabla \cdot (\varrho u_c) = 0 \tag{2.67}$$

with the macroscopic chemotactic velocity being

$$u_c = \frac{\phi}{(\phi + \psi)}v_c = \frac{\phi}{(\phi + \psi)}\frac{\nabla S}{|\nabla S|}. \tag{2.68}$$

In spite of the differences to our first kinetic model, the approximating equation for the macroscopic density is, in lowest order, again a convection equation. Importantly, the chemotactic velocity depends in both cases on the temporal derivative of S. Given that the functions ϕ and ψ are increasing and decreasing in S_t, respectively, the macroscopic chemotactic velocity here is larger for

positive values of the temporal derivative than for negative ones. Exposed to a wave of cAMP, the cells would naturally be prevented from following the wave back, which corresponds to the results of the discrete model in [8].

The model (2.67), (2.68) has to be handled with care, since the chemotactic velocity is discontinuous at stationary points of S. This leads to immediate cell concentration at maxima of S and to total depletion of cells around minima of S (see [43] for a theory of transport equations with discontinuous coefficients).

2.5 Conclusion

There already is a large history of modelling for Dd, and possible resolutions to the chemotactic wave paradox have been considered in mathematical models previously. A simple model based on an inhibitory mechanism is introduced in Rappel *et al.* [44]. The authors assume that in the presence of a cAMP wave, an intracellular, rapidly diffusing messenger substance is produced, which leads to the establishment of cell polarity. This assymetry between the front and the back of the cell might inhibit a directional change and thus prevent the cells from following the back of the wave.

In Höfer *et al.* [22], a modification of the Keller-Segel model considering adaption of the cellular response is presented. If the chemotactic sensitivity is proportional to the fraction of active receptors, cells get desensitized at the back of the wave, which is another possible resolution to the chemotactic wave paradox. In [23], the authors combine their model with the Martiel-Goldbeter model equations [30] for cAMP dynamics. It is shown numerically that their assumptions on the chemotactic sensitivity lead to cell aggregation, and the resulting patterns are investigated analytically.

Desensitation of cells has also been built into the discrete cell model by Dallon and Othmer [8] introduced in section 2.4. A theoretical analysis of the signal seen by the cells, again suggesting a mechanism based on space- and time-dependent intracellular gradients is discussed in [32].

In spite of the large effort that has been put into understanding the intracellular pathways and mechanisms in Dd both experimentally and theoretically, the whole machinery is still not completely understood and for other cell types even less is known. Although Dd can serve as a model organism up to some extent, chemotaxis models that are not based on specific knowledge concerning the internal dynamics are relevant. The kinetic models presented in this chapter are only based on the movement patterns of cells and the observation that slime molds seem to be able to assess the direction of a temporal gradient. Nevertheless, it turns out that our assumptions on the turning kernel are adequate to resolve the chemotactic wave paradox.

Chapter 3

The Keller-Segel model with small diffusivity

Motivated by the results from the last chapter, we investigate a macroscopic model for chemotaxis with small cell diffusivity. More precisely, we consider (1.1), (1.2) in one space dimension,

$$\varrho_t + (\chi(\varrho)\varrho S_x)_x = D\varrho_{xx}, \tag{3.1}$$

with $x \in (0, L)$ and $t > 0$. The diffusion D is assumed to be constant and the chemotactic sensitivity $\chi(\varrho)$ to be of the form

$$\chi(\varrho) = \chi_0 \left(1 - \frac{\varrho}{\varrho_{max}}\right), \tag{3.2}$$

the maximal cell density ϱ_{max} and χ_0 being positive constants. Thus, the chemotactic response of the cells is shut off when a maximal density is reached. The evolution of the chemoattractant S is described by

$$S_{xx} = \beta S - \alpha\varrho. \tag{3.3}$$

This elliptic equation, instead of the more frequently used parabolic equation, is appropriate if we assume that diffusion of the chemoattractant is large in relation to the characteristic time and length scales of the problem.

We non-dimensionalize the equations (3.1) and (3.3) by choosing reference values for time, length, cell density and the chemical concentration, respectively:

$$x_0 = \frac{1}{\sqrt{\beta}}, \quad t_0 = \frac{1}{\alpha\chi_0\varrho_{max}}, \quad \varrho_0 = \varrho_{max}, \quad S_0 = \frac{\alpha\varrho_{max}}{\beta}.$$

By introducing the dimensionless quantities

$$\bar{x} = \frac{x}{x_0}, \quad \bar{t} = \frac{t}{t_0}, \quad \bar{\varrho} = \frac{\varrho}{\varrho_0} \quad \text{and} \quad \bar{S} = \frac{S}{S_0}$$

and immediately dropping the bars, we obtain the non-dimensionalized system

$$\varrho_t + (\varrho(1 - \varrho)S_x)_x = \varepsilon\varrho_{xx} \tag{3.4}$$

$$S_{xx} = S - \varrho. \tag{3.5}$$

The only remaining dimensionless parameter is now

$$\varepsilon = \frac{D\beta}{\alpha\chi_0\varrho_{max}}.$$

and in the following, we will be concerned with $\varepsilon \ll 1$. The initial condition is given by

$$\varrho(x, 0) = \varrho_I. \tag{3.6}$$

We choose homogeneous Neumann boundary conditions, i.e.

$$\varrho_x(0, t) = \varrho_x(L, t) = 0, \quad S_x(0, t) = S_x(L, t) = 0. \tag{3.7}$$

In the next section, we will analyze the limit $\varepsilon \to 0$ of system (3.4), (3.5). By deriving estimates which are uniformly valid for $\varepsilon > 0$, we will, by a compactness argument, show convergence of ϱ and S to entropy solutions of the corresponding hyperbolic system,

$$\bar{\varrho}_t + (\bar{\varrho}(1 - \bar{\varrho})\bar{S}_x)_x = 0, \tag{3.8}$$

$$\bar{S}_{xx} = \bar{S} - \bar{\varrho}, \tag{3.9}$$

with

$$\bar{S}_x(0, t) = \bar{S}_x(L, t) = 0 \tag{3.10}$$

and subject to the initial condition

$$\bar{\varrho}(x, 0) = \bar{\varrho}_I. \tag{3.11}$$

As a consequence of (3.10), the characteristics of (3.8) are parallel to the boundary and no boundary conditions for $\bar{\varrho}$ are needed.

In section 3.2, we will study the long time behaviour of solutions of both the hyperbolic and the parabolic system. In the latter, the formation of so-called pseudo-stationary steady states can be observed. We will use formal asymptotics to derive a system of ordinary differential equations to describe the movement of these patterns. Finally, in section 3.3, we will investigate the long-time behaviour of solutions numerically.

3.1   Convergence of Solutions

In this section, we investigate the limit $\varepsilon \to 0$ in (3.4), (3.5), (3.6), (3.7). A similar problem from semiconductor physics is considered in Markowich and Szmolyan [29]. There, however, the non-linearity of the flux is only due to a coupling with an electric field (the equivalent to the chemical concentration here), and the formation of shocks in the hyperbolic problem is not observed.

The equations (3.4), (3.5) can be seen as a special case of the system analyzed in Hillen and Painter [21] (in particular, parabolic instead of elliptic equations for S are treated in [21]). The authors show the existence of an invariant region for (ϱ, S) in $\mathbb{R}^2$ and thus prove global existence of smooth solutions. In our case, the corresponding proof will be rather straightforward.

We make the following assumption on the initial data $\varrho_I(x) = \varrho(x, 0)$:

(A1) $\varrho_I \in W^{1,1}(0, L)$, $0 \le \varrho_I \le 1$, uniformly in ε.

Theorem 3
Let assumption (A1) hold. Then there exists a unique, global, smooth solution of (3.4), (3.5), (3.6), (3.7) satisfying

$$0 \le \varrho(x, t),\ S(x, t) \le 1 \quad \text{and} \quad \int_0^L \varrho(x, t)\, dx = \int_0^L \varrho_I(x)\, dx \tag{3.12}$$

and

$$S \in L^\infty((0, \infty); W^{2,\infty}(0, L)), \tag{3.13}$$

uniformly in ε as $\varepsilon \to 0$.

Proof. Local existence of smooth solutions can be shown by standard techniques (see for instance [39]). Then global existence follows from a comparison principle: writing (3.4) as

$$\varrho_t + (2\varrho - 1)S_x \varrho_x + \varrho(1 - \varrho)(S - \varrho) = \varepsilon \varrho_{xx},$$

it can be immediately seen that $\varrho = 0$ and $\varrho = 1$ are lower and upper solutions, respectively. The bounds for S are an obvious consequence of (3.5) and the maximum principle. We continue with estimates for the derivatives of ϱ.

Lemma 3
Let assumption (A1) hold. Then the solution of (3.4)-(3.7) satisfies

$$\varrho \in L^\infty_{loc}((0, \infty); W^{1,1}(0, L)), \quad \text{uniformly in } \varepsilon.$$

Proof. Differentiation of (3.4) with respect to x yields

$$\varrho_{xt} + ((1 - 2\varrho)\varrho_x S_x + \varrho(1 - \varrho)S_{xx})_x = \varepsilon \varrho_{xxx}. \tag{3.14}$$

We define an approximation of the sign function by $\sigma_\delta(z) = \sigma(z/\delta)$, $0 < \delta \ll 1$, with σ smooth, increasing, $\sigma(0) = 0$ and $\sigma(z) = \text{sign } z$ for $|z| > z_0$. Then, with $\text{abs}_\delta(z) := \int_0^z \sigma_\delta(\xi)d\xi$, the convergence of $\text{abs}_\delta(z)$ to $|z|$ as $\delta \to 0$ is uniform in $z \in \mathbb{R}$. Multiplying (3.14) with $\sigma_\delta(\varrho_x)$ and integrating with respect to x yields

$$\int_0^L \sigma_\delta(\varrho_x)\varrho_{xt} \, dx + \int_0^L \sigma_\delta(\varrho_x)(\varrho_x S_x(1 - 2\varrho))_x \, dx$$

$$+ \int_0^L \sigma_\delta(\varrho_x)(\varrho(1 - \varrho)(S - \varrho))_x \, dx = \varepsilon \int_0^L \sigma_\delta(\varrho_x)\varrho_{xxx} \, dx. \tag{3.15}$$

We integrate (3.15) by parts. The boundary terms vanish and we obtain

$$\frac{d}{dt} \int_0^L \text{abs}_\delta(\varrho_x) \, dx - \int_0^L \sigma_\delta'(\varrho_x)\varrho_x \varrho_{xx} S_x(1 - 2\varrho) \, dx$$

$$+ \int_0^L \sigma_\delta(\varrho_x)(\varrho(1 - \varrho)(S - \varrho))_x \, dx = -\varepsilon \int_0^L \sigma_\delta'(\varrho_x)\varrho_{xx}^2 \, dx \le 0. \tag{3.16}$$

The function $f_\delta(z) = \sigma_\delta(z)z - \text{abs}_\delta(z)$ satisfies $f_\delta'(z) = \sigma_\delta'(z)z$ and converges to 0 uniformly in $z \in \mathbb{R}$. We integrate the second term in (3.16) by parts, which gives

$$\frac{d}{dt} \int_0^L \text{abs}_\delta(\varrho_x) \, dx \le - \int_0^L f_\delta(\varrho_x)(S_x(1 - 2\varrho))_x \, dx$$

$$- \int_0^L \sigma_\delta(\varrho_x)(\varrho(1 - \varrho)(S - \varrho))_x \, dx. \tag{3.17}$$

The last term can be estimated by

$$- \int_0^L \sigma_\delta(\varrho_x)(\varrho(1 - \varrho)(S - \varrho))_x \, dx = - \int_0^L \sigma_\delta(\varrho_x)\varrho(1 - \varrho)S_x \, dx$$

$$- \int_0^L \sigma_\delta(\varrho_x)\varrho_x(3\varrho^2 - 2\varrho(S + 1) + S) \, dx \le c_1 + c_2 \int_0^L |\varrho_x| \, dx.$$

In the limit $\delta \to 0$, the first term of the right hand side of (3.17) vanishes and we obtain

$$\frac{d}{dt} \int_0^L |\varrho_x| \, dx \le c_1 + c_2 \int_0^L |\varrho_x| dx. \tag{3.18}$$

The assertion of lemma 3 now follows from the Gronwall inequality. $\quad\square$

Lemma 4

Let (A1) hold. Then the solution of (3.4)-(3.7) satisfies

$$\sqrt{\varepsilon}\varrho_x, S_{xt} \in L^2_{loc}((0,\infty) \times [0,L]), \quad \text{uniformly in } \varepsilon.$$

Proof. We write (3.4) as

$$\varrho_t = (\varepsilon\varrho_x - \varrho(1-\varrho)S_x)_x. \tag{3.19}$$

Multiplication by ϱ and integration with respect to x leads to

$$\frac{1}{2}\frac{d}{dt}\int_0^L \varrho^2\, dx + \varepsilon\int_0^L \varrho_x^2\, dx = \int_0^L \varrho(1-\varrho)S_x\varrho_x\, dx. \tag{3.20}$$

Since the integrand in the last term is in $L^1((0,L))$ uniformly in t and ε by the previous result, we obtain the boundedness of $\sqrt{\varepsilon}\varrho_x$ by integration with respect to t. As a consequence, the flux density $J = \varrho(1-\varrho)S_x - \varepsilon\varrho_x$ is also uniformly bounded in $L^2_{loc}((0,\infty) \times [0,L])$. Differentiating equation (3.5) with respect to x and t and using $\varrho_t + J_x = 0$, we obtain

$$S_{xxxt} - S_{xt} = J_{xx}.$$

Thus, $S_{xt} = (\partial_x^2 - 1)^{-1}\partial_x^2 J$. Since the expression on the right hand side is a bounded operator applied to a function in $L^2_{loc}((0,\infty) \times [0,L])$, the proof is complete. $\square$

Theorem 4

Let the assumption (A1) hold, (ϱ, S) be a solution of (3.4) - (3.7), and $T > 0$. Then, as $\varepsilon \to 0$ (restricting to subsequences),

$$\varrho \to \bar{\varrho} \text{ in } C([0,T]; L^1((0,L))) \quad \text{and} \quad S \to \bar{S} \text{ in } C([0,T]; C^1([0,L])). \tag{3.21}$$

The limit $(\bar{\varrho}, \bar{S}) \in L^\infty((0,T); BV((0,L)) \times W^{2,\infty}((0,L)))$ solves (3.8), (3.9), (3.10), where $\bar{\varrho}_I \in BV((0,L))$ is an accumulation point of ϱ_I. Moreover, $\bar{\varrho}$ is an entropy solution of (3.8), i.e.

$$\eta(\bar{\varrho})_t + (\psi(\bar{\varrho})\bar{S}_x)_x + (\bar{\varrho}(1-\bar{\varrho})\eta'(\bar{\varrho}) - \psi(\bar{\varrho}))(\bar{S} - \bar{\varrho}) \leq 0 \tag{3.22}$$

holds in the weak sense for every smooth, convex η and with $\psi'(\bar{\varrho}) = (1 - 2\bar{\varrho})\eta'(\bar{\varrho})$.

Remark: Note that the entropy inequality does not give rise to a decaying entropy functional.

Proof. The boundedness of the flux density (proof of lemma 4) gives $\varrho_t \in L^2((0,T); H^{-1}((0,L)))$. Together with lemma 3 this implies that ϱ is in a compact set in $C([0,T]; L^1((0,L)))$ (see Simon [47]). From theorem 3, lemma 4 and an anisotropic generalization of the Sobolev embedding of $W^{1,p}$ in $C^{0,1-n/p}$, $p > n$ (see Haskovec and Schmeiser [16]), it follows that S_x is uniformly bounded in $C^{0,1/3}([0,T] \times \bar{\Omega})$, $T > 0$. An application of the Arzela-Ascoli theorem concludes the proof of (3.21). The strong convergence of ϱ and S_x allows to pass to the limit in the weak formulation of (3.4)-(3.7) giving the weak formulation of (3.8)-(3.10) for $\bar{\varrho}$ and $\bar{S}$. The entropy inequality (3.22) follows analogously. □

3.2 Asymptotic behaviour of solutions

3.2.1 Long-time behaviour of the hyperbolic system

In this section, we investigate the stability and the asymptotic behaviour of entropy solutions of the hyperbolic system. Stationary solutions of (3.8), (3.9), (3.10) satisfy

$$\bar{\varrho}(1 - \bar{\varrho})\bar{S}_x = 0 \tag{3.23}$$

$$\bar{S}_{xx} = \bar{S} - \bar{\varrho}. \tag{3.24}$$

It can be immediately seen that $\bar{\varrho} = \bar{S} = const$ is a solution.

Lemma 5
The constant solution, $\bar{\varrho} = \bar{S} = \frac{m}{L}$, where $0 < m < L$ is the total mass, of system (3.8), (3.9), (3.10) is unstable.

Proof. We multiply (3.8) by $\bar{S}$ and differentiate (3.9) with respect to t to obtain

$$\frac{1}{2}\frac{d}{dt}\int_0^L (\bar{S}^2 + \bar{S}_x^2)dx = \int_0^L \bar{\varrho}(1 - \bar{\varrho})\bar{S}_x^2 dx. \tag{3.25}$$

For small non constant perturbations, the right hand side of this equation is positive $\forall t$, hence $\int_0^L (\bar{S}^2 + \bar{S}_x^2)dx$ is increasing in time. We rearrange this integral by writing

$$\int_0^L (\bar{S}^2 + \bar{S}_x^2)dx = \int_0^L \left[\left(\frac{m}{L} + \bar{S} - \frac{m}{L}\right)^2 + \bar{S}_x^2\right]dx \tag{3.26}$$

$$= \frac{m^2}{L} + 2\int_0^L \frac{m}{L}\left(\bar{S} - \frac{m}{L}\right)dx + \int_0^L \left[\left(\bar{S} - \frac{m}{L}\right)^2 + \bar{S}_x^2\right]dx.$$

Since the total mass is conserved, we consider only perturbations with mass 0. Thus, we have $\int_0^L \bar{S}\,dx = \int_0^L \bar{\varrho}\,dx = m \ \forall\ t$, and the second term on the right hand side vanishes. Hence,

$$\min_{\int \bar{S}dx=m} \int_0^L \left(\bar{S}^2 + \bar{S}_x^2\right)dx = \frac{m^2}{L},$$

which is only achieved for $\bar{S} = \frac{m}{L}$. As the integral on the left hand side is increasing in time, lemma 5 follows. □

Lemma 6
As $t \to \infty$, $\bar{\varrho}(1 - \bar{\varrho})\bar{S}_x^2 \to 0$ in the following sense:

$$\int_\tau^\infty \int_0^L \bar{\varrho}(1 - \bar{\varrho})\bar{S}_x^2 dx\,dt \xrightarrow{\tau \to \infty} 0. \tag{3.27}$$

Proof. Integration of (3.25) from $t = 0$ to ∞ shows that

$$\int_0^\infty \int_0^L \bar{\varrho}(1 - \bar{\varrho})\bar{S}_x^2 dx dt < \infty, \tag{3.28}$$

which implies the assertion. □

From this, and the steady state equations (3.23), (3.24), we expect convergence to piecewise constant steady states, with $\bar{\varrho} = 0$, $\bar{\varrho} = 1$ or $\bar{S}_x = 0$. Going back to the time-dependent problem (3.8), (3.9) and applying the method of characteristics, we find that along characteristics given by $\dot{x} = (1 - 2\bar{\varrho})\bar{S}_x$, $\bar{\varrho}$ evolves according to $\dot{\bar{\varrho}} = (\bar{\varrho} - \bar{S})\bar{\varrho}(1 - \bar{\varrho})$. It immediately follows that $\bar{\varrho} = \bar{S} = const$, with $0 < const < 1$, is unstable. If $\bar{\varrho}$ gets sufficiently small such that $\bar{S} > \bar{\varrho}$, then $\bar{\varrho} = 0$ is attracting, and a similar argument holds for $\bar{\varrho} = 1$. Hence, we expect solutions to approach (as $t \to \infty$) functions of the form

$$\bar{\varrho}_\infty(x) = \begin{cases} 1 & x \in P := \bigcup(x_{2k-1}, x_{2k}), \quad 1 \leq k \leq N \\ 0 & x \in Z := (0, L)\backslash P \end{cases} \tag{3.29}$$

with $0 \leq x_1 < x_2 < ... < x_{2N} \leq L$ and

$$\bar{S}_{\infty,xx} = \bar{S}_\infty - \bar{\varrho}_\infty, \quad \bar{S}_{\infty,x} = 0 \quad \text{at} \quad x = 0, L. \tag{3.30}$$

Clearly, not all possible stationary solutions $\bar{\varrho}_\infty$ are indeed entropy solutions. In order to derive an entropy condition, we consider a stationary solution of the form

$$\bar{\varrho}_\infty = \begin{cases} 0 & x < a \\ 1 & x > a, \end{cases} \tag{3.31}$$

for some $0 < a < L$. Then, the entropy inequality (3.22) becomes

$$(\psi(\bar{\varrho}_\infty)\bar{S}_{\infty,x})_x \leq \psi(\bar{\varrho}_\infty)(\bar{S}_\infty - \bar{\varrho}_\infty). \tag{3.32}$$

We multiply (3.32) by a smooth testfunction $\varphi_k(x,t)$ chosen such that as $k \to \infty$, φ_k approaches a function that is 1 in the interval $(a - \varepsilon, a + \varepsilon)$ and zero everywhere else. Integrating (3.32) by parts and letting $k \to \infty$ yields

$$\psi(\bar{\varrho}_\infty)\bar{S}_{\infty,x}\Big|_{x=a+\varepsilon} \leq \psi(\bar{\varrho}_\infty)\bar{S}_{\infty,x}\Big|_{x=a-\varepsilon} + \int_{a-\varepsilon}^{a+\varepsilon} \psi(\bar{\varrho}_\infty)(\bar{S} - \bar{\varrho}_\infty)\,dx. \tag{3.33}$$

We specify the entropy flux by $\psi(\bar{\varrho}_\infty) = \frac{\bar{\varrho}_\infty^2}{2} - \frac{2\bar{\varrho}_\infty^3}{3}$ (this corresponds to choosing the entropy $\eta(\bar{\varrho}_\infty) = \frac{\bar{\varrho}_\infty^2}{2}$). Then, if $\bar{S}_{\infty,x}(a) \neq 0$, we let $\varepsilon \to 0$ in (3.33) to obtain the inequality $\bar{S}_{\infty,x}(a) > 0$. Similarly, considering a stationary solution $\bar{\varrho}_\infty$ with a jump from 1 to 0 leads to the inequality $\bar{S}_{\infty,x}(a) < 0$.

If $\bar{S}_{\infty,x}(a) = 0$, we use the Taylor expansion $\bar{S}_{\infty,x}(a \pm \varepsilon) = \pm\bar{S}_{\infty,xx}(a\pm)\varepsilon + \mathcal{O}(\varepsilon^2)$ in equation (3.33). Dividing by ε yields, after using (3.9) and letting $\varepsilon \to 0$, the relation $1 - \bar{S}_\infty(a) \leq 0$. Obviously, this inequality can never be fulfilled, and hence, a jump of $\bar{\varrho}_\infty$ is not allowed if $\bar{S}_{\infty,x} = 0$ at the jump location. Summarizing these results, it follows that for an arbitrary number of jumps of $\bar{\varrho}_\infty$, the asymptotic solution $\bar{S}_\infty$ has to satisfy

$$(-1)^i \bar{S}_{\infty,x}(x_i) < 0, \quad 1 \leq i \leq 2N. \tag{3.34}$$

Furthermore, it follows from mass conservation that

$$\sum_{k=1}^{N}(x_{2k} - x_{2k-1}) = \int_0^L \bar{\varrho}_I\,dx.$$

Next, we investigate the stability of the stationary solution $(\bar{\varrho}_\infty, \bar{S}_\infty)$ with respect to a particular class of perturbations. We introduce the initial data

$$\bar{\varrho}_I(x) = \begin{cases} 1 + \varepsilon u_I(x) & x \in (x_{2k-1} + \varepsilon\xi_{2k-1}(0), x_{2k} + \varepsilon\xi_{2k}(0)) = I_k(0) \\ \varepsilon u_I(x) & \text{else,} \end{cases}$$
$$\tag{3.35}$$

where u_I is a piecewise smooth function and $|\varepsilon| \ll 1$. Then, solutions of (3.8), (3.9) have jumps at $x_i + \varepsilon\xi_i(t)$, and

$$\bar{\varrho}(x,t) = \begin{cases} 1 + \varepsilon u(x,t) & x \in \bigcup I_k(t) \\ \varepsilon u(x,t) & \text{else.} \end{cases} \tag{3.36}$$

The Rankine-Hugoniot jump condition reads

$$\varepsilon\dot{\xi}_i[\bar{\varrho}] = [\bar{\varrho}(1 - \bar{\varrho})\bar{S}_x]\Big|_{x=x_i+\varepsilon\xi_i}$$

which in leading order yields

$$\dot{\xi}_i(t) = -\left(u(x_i+, t) + u(x_i-, t)\right) \bar{S}_{\infty,x}(x_i).$$

Using (3.36) in (3.8), it follows that $u(x, t)$ approximately satisfies

$$
\begin{aligned}
u_t - (u\bar{S}_{\infty,x})_x &= 0 \quad \text{in} \quad P \\
u_t + (u\bar{S}_{\infty,x})_x &= 0 \quad \text{in} \quad Z.
\end{aligned}
$$

By the method of characteristics, we derive

$$\dot{x} = -\bar{S}_{\infty,x}, \quad \dot{u} = u\bar{S}_{\infty,xx} = u(\bar{S}_\infty - 1) \quad \text{in} \quad P$$

$$\dot{x} = \bar{S}_{\infty,x}, \quad \dot{u} = -u\bar{S}_{\infty,xx} = -u\bar{S}_\infty \quad \text{in} \quad Z.$$

Since $\bar{S}_\infty$ is concave in P and convex in Z, exactly one extremum $x_{i+\frac{1}{2}}$ exists between x_i and x_{i+1}. All of the characteristics except those starting at $x_{i+\frac{1}{2}}$ go into one of the x_i, and u decays along characteristics. The length of the kth plateau for $t \to \infty$ is given by

$$
\begin{aligned}
l(I_k(\infty)) &= l(I_k(0)) + \varepsilon \int_0^\infty \left(\dot{\xi}_{2k} - \dot{\xi}_{2k-1} \right) dt \\
&= l(I_k(0)) + \varepsilon \int_0^\infty [-(u\bar{S}_{\infty,x})(x_{2k}+) - (u\bar{S}_{\infty,x})(x_{2k}-) \\
&\quad + (u\bar{S}_{\infty,x})(x_{2k-1}+) + (u\bar{S}_{\infty,x})(x_{2k-1}-)]dt \\
&= l(I_k(0)) - \varepsilon \int_0^\infty \int_{x_{2k-1}}^{x_{2k}} (u\bar{S}_{\infty,x})_x dx dt + \varepsilon \int_0^\infty \int_{x_{2k}}^{x_{2k+1/2}} (u\bar{S}_{\infty,x})_x dx dt \\
&\quad + \varepsilon \int_0^\infty \int_{x_{2k-3/2}}^{x_{2k-1}} (u\bar{S}_{\infty,x})_x dx dt \\
&= l(I_k(0)) - \varepsilon \int_{x_{2k-1}}^{x_{2k}} u\Big|_{t=0}^\infty dx - \varepsilon \int_{x_{2k}}^{x_{2k+1/2}} u\Big|_{t=0}^\infty dx - \varepsilon \int_{x_{2k-3/2}}^{x_{2k-1}} u\Big|_{t=0}^\infty dx
\end{aligned}
$$

Since $u \xrightarrow{t\to\infty} 0$, we obtain

$$l(I_k(\infty)) = l(I_k(0)) + \varepsilon \int_{x_{2k-3/2}}^{x_{2k+1/2}} u_I dx. \tag{3.37}$$

Thus, as $t \to \infty$, each plateau gets all the mass initially distributed between the neighbouring minima of $\bar{S}_\infty$. We can interpret this as a neutral stability of the N plateau steady state with respect to perturbations of the type (3.35).

(a) $t = 15$ (b) $t = 25$ (c) $t = 35$

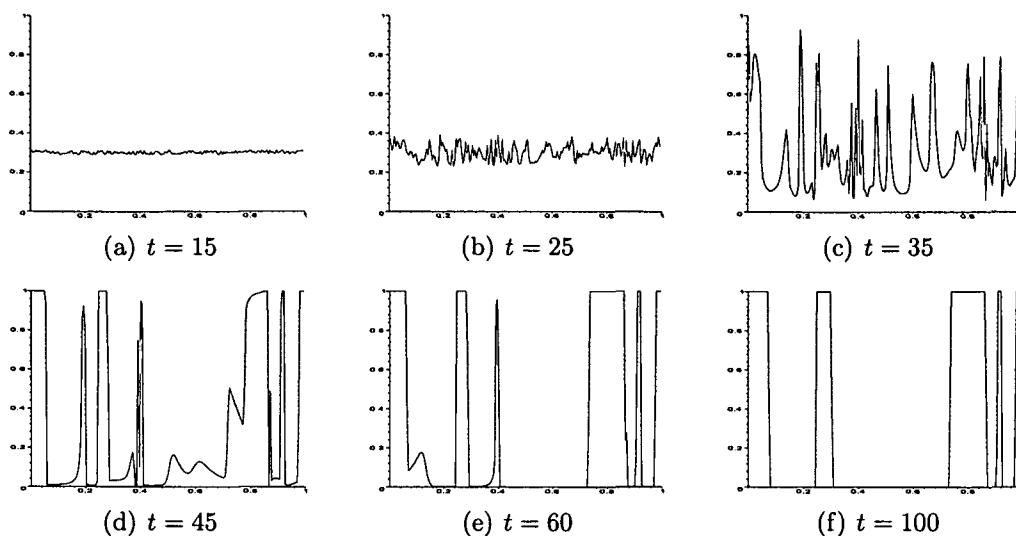(d) $t = 45$ (e) $t = 60$ (f) $t = 100$

Figure 3.1: Temporal evolution of the cell density $\bar{\varrho}$, starting from random initial data $\bar{\varrho}_I \in [0.3, 0.31]$ and with $L = 1$.

In Fig. 3.1 and 3.2, we solved the problem (3.8) - (3.10) numerically. At each time step, first the new chemical concentration is calculated from the old cell density, then the cell density is updated using an upwind method. In Fig. 3.1, we can observe the formation of shocks and rarefaction waves, until, in the last picture, the stationary state is reached and no further movement of the plateaus can be observed. In Fig. 3.2, the corresponding chemical concentration $\bar{S}$ is shown. Note that as discussed above, the chemical follows the course of the cell density $\bar{\varrho}$, even in the case of the slim plateau on the right side of the domain.

3.2.2 Long-time behaviour of the parabolic system

In this section, we will be concerned with the stability and the asymptotic behaviour of solutions of the parabolic system. Now, stationary solutions are given by

$$\varrho(1 - \varrho)S_x - \varepsilon\varrho_x = 0 \tag{3.38}$$

$$S_{xx} = S - \varrho. \tag{3.39}$$

Typically, either stationary solutions themselves or the solutions together with their reflection with respect to one of the boundaries are periodic. In Popatov and Hillen [41], the long-time behaviour of a similar system of equations is
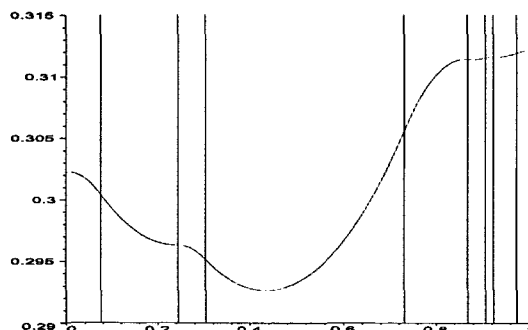
Figure 3.2: Cell density $\bar{\varrho}$ (dark) and chemical concentration $\bar{S}$ (light) at $t = 100$.

studied. The main difference to the system considered here is that in [41], S is given by a parabolic equation and that the diffusivity of ϱ is assumed to be $\mathcal{O}(1)$. The authors study bifurcations from the spatially uniform stationary solution in dependence of a bifurcation parameter inversely proportional to ε. It turns out that the constant solution can be stabilized by adding enough diffusivity. After a first bifurcation its stability is transferred to a bifurcating solution. Related to these results is

Lemma 7

The constant solution of system (3.4), (3.5) is stable for $\varepsilon > \frac{1}{4}$.

Proof. Similarly to the proof of lemma 5, we multiply (3.4) with S and differentiate (3.5) with respect to t to obtain, after integration by parts of the last term on the right hand side,

$$\frac{1}{2}\frac{d}{dt}\int_0^L (S^2 + S_x^2)dx = \int_0^L \varrho(1 - \varrho)S_x^2 dx - \varepsilon \int_0^L (S_x^2 + S_{xx}^2)dx. \qquad (3.40)$$

We can estimate the left hand side by

$$\frac{1}{2}\frac{d}{dt}\int_0^L (S^2 + S_x^2)dx = \int_0^L \varrho(1 - \varrho)S_x^2 dx - \varepsilon \int_0^L (S_x^2 + S_{xx}^2)dx \qquad (3.41)$$

$$\leq \left(\frac{1}{4} - \varepsilon\right)\int_0^L (S_x^2 + S_{xx}^2)dx.$$

For $\varepsilon > \frac{1}{4}$, the right hand side of (3.41) is negative. Integration from 0 to t yields

$$\int_0^L S_x^2(x,t)\,dx \leq \left(\frac{1}{2} - 2\varepsilon\right)\int_0^t\int_0^L S_x^2 dx + \int_0^L (S^2 + S_x^2)dx\bigg|_{t=0}.$$

Applying Gronwall's lemma, it follows that $\|S_x\|_{L^2(0,L)} \to 0$ and as a consequence, $S \to const$ as $t \to \infty$. $\square$

Fig. 3.3 shows the numerical solution of system (3.4) - (3.7) with $\varepsilon = 2 \times 10^{-4}$. We used the same numerical scheme as in the previous section with an explicit discretization of the diffusion term. Starting from homogeneous initial data with small perturbations, a pattern with several plateaus is formed as for the hyperbolic problem. Once this pattern has formed, it remains structurally stable for a long time, with the plateaus moving very slowly. Eventually, neighbouring plateaus merge with each other. This merging process occurs on a comparatively fast time scale. The new pattern, now with one peak less, undergoes the same coarsening process.

Experimentally, this so called metastable behaviour is a well known phenomenon in many fields, for instance solid-state physics. Mathematically, it has been studied in various contexts such as the movement of viscous shocks [28], [45] or the Cahn-Hillard equation (for instance [3] and [4]). A chemotaxis model featuring the formation of spike solutions is considered in [48].

The peculiar long-time behaviour of system (3.4), (3.5) can be interpreted as follows. Each pseudo-stationary state of the parabolic system is exponentially close to a stationary entropy solution of the hyperbolic system. In contrast to the latter however, the small diffusion allows plateaus to communicate with each other, and smaller plateaus are attracted by neighbouring larger ones producing more chemoattractant. The whole phenomenon depends on a non-zero diffusion coefficient ε. Eventually, plateaus will get so close to each other that in general, the corresponding stationary solutions of the hyperbolic system cannot satisfy the entropy condition any more. Then, a fast transition takes place and the smaller plateau merges with the larger one. On this fast time scale, solutions behave practically like in the hyperbolic case, and a smoothened version of a rarefaction wave can be observed.

After the two peaks have merged, it is again diffusion that dominates the behaviour. The whole process repeats itself, until only one single plateau is left, which will typically move to one of the domain boundaries. Thus, the only stable stationary state seems to be one plateau at the left or right boundary of the domain.

By construction of approximate solutions, it is shown numerically and analytically in [41] that the eigenvalues describing the slow movement of the peaks exponentially approach zero as the length of the domain increases. These exponentially small eigenvalues are typical features of metastable systems. The authors also derive an ODE describing the dynamics of a structure with two plateaus at the domain boundaries. Here, we will use exponential asymptotics to formally derive a system of ordinary differential equations describing the

(a) $t = 125$ (b) $t = 175$ (c) $t = 225$
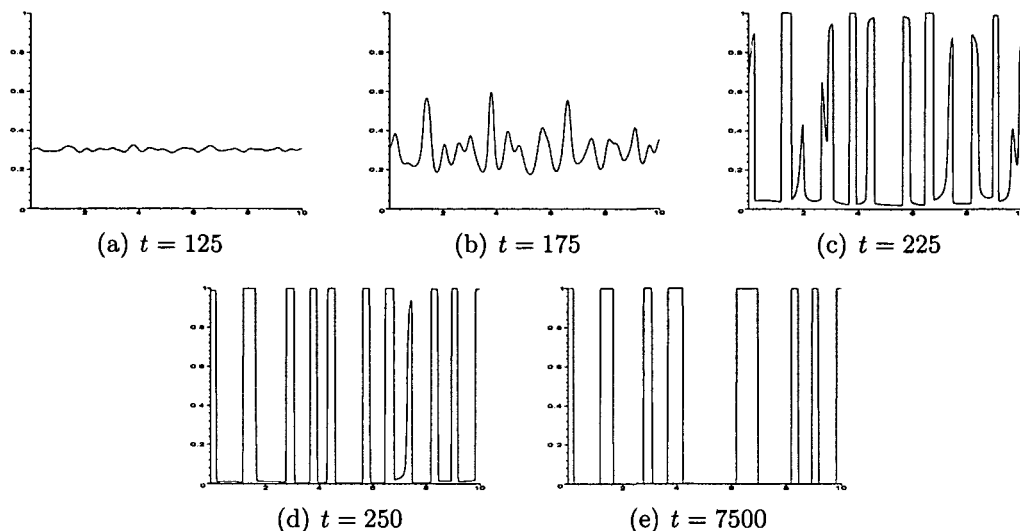

(d) $t = 250$ (e) $t = 7500$

Figure 3.3: Numerical solution of the parabolic system (3.4), (3.5) with random initial data $\varrho_I \in [0.3, 0.31]$, $L = 10$ and $\varepsilon = 2 \times 10^{-4}$.

slow movement of the plateaus. This method has been successfully used in various applications, see for instance Ward [57] and references therein.

Metastable dynamics of the parabolic system

In the following analysis of the long-time behaviour of system (3.4), (3.5), we will assume that the formation of patterns from the initial data has already taken place, and that a quasi-stationary pattern with N plateaus has formed. Our aim will be to derive a system of equations describing the evolution of the positions of the plateau boundaries.

A first approximation to a solution of the parabolic problem with N plateaus is the stationary solution of the hyperbolic problem $(\bar{\varrho}_\infty, \bar{S}_\infty)$ solving (3.29) and (3.30). However, we change the numbering of the plateau boundaries, counting only interior ones: $0 < x_1 < \ldots < x_M < L$ with $2N - 2 \leq M \leq 2N$. For a better approximation, we introduce the boundary layer variables

$$\eta_i = \frac{x - x_i}{\varepsilon}, \quad i = 1, \ldots, M \tag{3.42}$$

at each point x_i where $\bar{\varrho}_\infty$ is discontinuous. Then, for each boundary layer, we obtain from (3.38) an equation of the form

$$\frac{d\hat{\varrho}_i}{d\eta} = \hat{\varrho}_i(1 - \hat{\varrho}_i)S'(x_i) \tag{3.43}$$

where $S_x(x) = S_x(x_i + \varepsilon \eta_i)$ is approximated by $S'(x_i) := \bar{S}_{\infty,x}(x_i)$. The solution can be calculated explicitly,

$$\hat{\varrho}_i(\eta_i) = \frac{1}{1 + ce^{-S'(x_i)\eta_i}} \tag{3.44}$$

If we fix the solution such that $\hat{\varrho}_i(0) = \frac{1}{2}$, then $c = 1$. The shape of $\hat{\varrho}$ depends on the sign of $S'(x_i)$: for $S'(x_i) > 0$, $\hat{\varrho} \to 1$ as $\eta_i \to \infty$ and $\hat{\varrho} \to 0$ as $\eta_i \to -\infty$, for $S'(x_i) > 0$, the opposite holds. Thus, an appropriate boundary layer solution can be constructed for jumps satisfying the entropy condition (3.34). We now construct an approximate solution with N plateaus by

$$\tilde{\varrho}(x; x_1, ..., x_M) = \sum_{i=1}^{M} \hat{\varrho}_i \left(\frac{x - x_i}{\varepsilon} \right) - (M - N), \tag{3.45}$$

and

$$\tilde{S}_{xx} = \tilde{S} - \tilde{\varrho}, \quad \tilde{S}_x = 0 \text{ at } x = 0, L.$$

Note that $\tilde{S}$ and $\tilde{S}_x$ are uniformly (in x) close to $\bar{S}_\infty$ and $\bar{S}_{\infty,x}$, respectively.

Fundamental for the following asymptotics is the assumption that this approximate solution depends on time only through the positions of the boundary layers. Therefore, we write the exact solution $\varrho(x, t)$ as

$$\varrho(x, t) = \tilde{\varrho}(x; x_1(t), ..., x_M(t)) + r(x, t), \tag{3.46}$$

with $r \ll \tilde{\varrho}$ and, additionally, $r_t \ll \tilde{\varrho}_t$. Boundary conditions for r are given by

$$r_x = -\tilde{\varrho}_x \text{ at } x = 0, L. \tag{3.47}$$

The corresponding ansatz for S is

$$S(x, t) = \tilde{S}(x, t) + \sigma(x, t). \tag{3.48}$$

Then σ satisfies

$$\sigma_{xx} = \sigma - r, \quad \sigma_x = 0 \text{ at } x = 0, L.$$

Thus, we can write σ as

$$\sigma[r] = \int_0^L G(x, y)r(y)dy, \tag{3.49}$$

with an appropriate Greens's function $G(x, y)$ (which is symmetric in x and y). An approximate version of (3.4), (3.5) can now be written as

$$\mathcal{L}r = h := \tilde{\varrho}_t - \varepsilon\tilde{\varrho}_{xx} + (\tilde{\varrho}(1 - \tilde{\varrho})\tilde{S}_x)_x \tag{3.50}$$

with

$$\mathcal{L}r = \varepsilon r_{xx} - \left[(1 - 2\tilde{\varrho})\tilde{S}_x r + \tilde{\varrho}(1 - \tilde{\varrho})\sigma[r]_x\right]_x. \tag{3.51}$$

Here the time derivative r_t has been dropped according to our assumptions together with quadratic terms in r. Multiplying (3.50) by a test function $\psi(x, t)$ and integrating we obtain

$$\begin{aligned}
\varepsilon(\psi r_x - \psi_x r)\Big|_0^L &+ \varepsilon \int_0^L \psi_{xx} r \, dx + \int_0^L r(1 - 2\tilde{\varrho})\tilde{S}_x \psi_x \, dx \\
&+ \int_0^L \tilde{\varrho}(1 - \tilde{\varrho})\sigma[r]_x \psi_x \, dx = \int_0^L h\psi \, dx.
\end{aligned} \tag{3.52}$$

With (3.49), the last term on the left hand side of (3.52) can be written as

$$\int_0^L \tilde{\varrho}(1 - \tilde{\varrho})\sigma[r]_x \psi_x \, dx = \int_0^L \int_0^L \tilde{\varrho}(1 - \tilde{\varrho})G_x(x, y)r(y)\psi_x \, dy \, dx. \tag{3.53}$$

We exchange x and y and integrate by parts. Using the symmetry of the Green's function $G(x, y) = G(y, x)$ yields

$$\begin{aligned}
\int_0^L \int_0^L &\tilde{\varrho}(1 - \tilde{\varrho})G_x(x, y)r(y)\psi_x \, dy \, dx \\
&= -\int_0^L r(x) \int_0^L G(y, x)(\tilde{\varrho}(1 - \tilde{\varrho})\psi_y(y))_y \, dy \, dx \\
&\quad + \int_0^L r(x)G(y, x)\tilde{\varrho}(1 - \tilde{\varrho})\psi_y(y)\Big|_0^L \, dx \\
&= -\int_0^L r(x)\frac{d}{dx} \int_0^L G(x, y)\tilde{\varrho}(1 - \tilde{\varrho})\psi_y \, dy \, dx + \sigma\psi_x\tilde{\varrho}(1 - \tilde{\varrho})\Big|_0^L \\
&= -\int_0^L r(x)\varphi[\psi]_x(x) \, dx + \sigma\psi_x\tilde{\varrho}(1 - \tilde{\varrho})\Big|_0^L
\end{aligned}$$

where $\varphi[\psi]$ solves

$$\varphi_{xx} = \varphi - \tilde{\varrho}(1 - \tilde{\varrho})\psi_x, \quad \varphi_x = 0 \text{ at } x = 0, L. \tag{3.54}$$

Hence we conclude

$$\begin{aligned}
\int_0^L \mathcal{L}r\psi \, dx &= \varepsilon(\psi r_x - \psi_x r)\Big|_0^L + \varepsilon \int_0^L \psi_{xx} r \, dx \\
&+ \int_0^L r(1 - 2\tilde{\varrho})\tilde{S}_x \psi_x \, dx - \int_0^L r\varphi[\psi]_x \, dx.
\end{aligned}$$

In order to dispose of the left hand side in (3.52) containing the unknown residual r, we choose for ψ approximate solutions of the adjoint problem

$$\mathcal{L}^*\psi = \varepsilon\psi_{xx} + (1 - 2\tilde{\varrho})\tilde{S}_x\psi_x - \varphi[\psi]_x = 0 \qquad (3.55)$$

together with the homogeneous Neumann boundary conditions

$$\psi_x = 0 \text{ at } x = 0, L. \qquad (3.56)$$

Then, considering the boundary conditions (3.47), equation (3.52) becomes

$$\int_0^L \tilde{\varrho}_t\psi \, dx = \varepsilon \int_0^L \tilde{\varrho}_{xx}\psi \, dx - \int_0^L (\tilde{\varrho}(1 - \tilde{\varrho})\tilde{S}_x)_x\psi \, dx - \varepsilon\psi\tilde{\varrho}_x\Big|_0^L. \qquad (3.57)$$

Similarly to the construction of $\tilde{\varrho}$ above, ψ will be constructed by combining several boundary layer solutions.

We will approximate (3.55) by disregarding the last term (this will be justified below) and by replacing $\tilde{S}_x$ by $\bar{S}_{\infty,x}$. The chemoattractant density $\bar{S}_\infty$ has in general $M - 1$ interior extrema $\bar{x}_1, ..., \bar{x}_{M-1}$ with the ordering $0 =: \bar{x}_0 < x_1 < \bar{x}_1 < x_2 < ... < \bar{x}_{M-1} < x_M < \bar{x}_M := L$. An interesting behaviour of solutions can be expected near these extrema and near the boundary layer positions x_i, where $\tilde{\varrho} \approx \frac{1}{2}$. At these turning points, the factor in front of ψ_x in (3.55) changes its sign. In the vicinity of $x = x_i$, solutions are decreasing for $x < x_i$ and increasing for $x > x_i$. Near $x = \bar{x}_i$, the opposite is the case. Thus, it can be anticipated that ψ_x is a so-called spike-layer solution: it is large only in the vicinity of the extrema of $\bar{S}_\infty$, and small everywhere else .

This gives an a posteriori justification for our decision to neglect the term φ_x in equation (3.55): the term $\tilde{\varrho}(1 - \tilde{\varrho})$ is exponentially small at extrema of $\bar{S}_\infty$, which means that the function φ as a solution of (3.54) is exponentially small everywhere.

We approximate $\bar{S}_{\infty,x}$ close to its extrema $\bar{x}_1, ..., \bar{x}_{M-1}$ by linear functions

$$\bar{S}_{\infty,x} \approx \bar{S}_{\infty,xx}(x = \bar{x}_i)(x - \bar{x}_i), \text{ for } |x - \bar{x}_i| \ll 1..$$

Near minima of $\tilde{S}$, $\tilde{\varrho}$ is very close to 0, around maxima it is close to 1. Simplifying (3.55) according to our observations, we obtain M layer equations of the form

$$\frac{d^2}{dz_i^2}\hat{\psi}_i + a_i z_i \frac{d\hat{\psi}_i}{dz_i} = 0, \qquad a_i := \left|\bar{S}_{\infty,xx}(x = \bar{x}_i)\right|, \qquad (3.58)$$

with the solutions

$$\hat{\psi}_i = \hat{\psi}_i(-\infty) + c\sqrt{\frac{\pi}{2a_i}}\left(1 + \text{erf}\left(\sqrt{\frac{a_i}{2}}z_i\right)\right). \qquad (3.59)$$
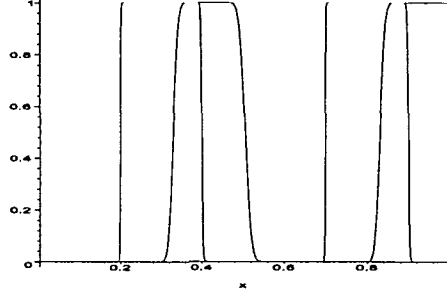
Figure 3.4: Example for an approximate solution $\tilde{\varrho}$ with two plateaus for $\varepsilon = 5 \times 10^{-5}$ and the functions ψ_2, ψ_4.

Thus, $\hat{\psi}_i$ varies rapidly in a boundary layer of thickness $\mathcal{O}(\sqrt{\varepsilon})$ and is almost constant everywhere else. If we fix $\hat{\psi}_i(\bar{x}_i) = \frac{1}{2}$ and $\hat{\psi}_i(-\infty) = 0$, $\hat{\psi}_i(\infty) = 1$ or vice versa, we obtain two sets of M boundary layer solutions,

$$\hat{\psi}_i^+(z_i) = \frac{1}{2}\left(1 + \operatorname{erf}\left(\sqrt{\frac{a_i}{2}}z_i\right)\right), \quad \hat{\psi}_i^-(z_i) = \frac{1}{2}\left(1 - \operatorname{erf}\left(\sqrt{\frac{a_i}{2}}z_i\right)\right),$$

with $i = 1, ..., M$. Each of these functions solves the original equation (3.55) up to exponentially small terms. Finally, we combine two of these boundary layer solutions at a time such that

$$\psi_i = \hat{\psi}_{i-1}^+(z_{i-1}) + \hat{\psi}_i^-(z_i) - 1, \quad i = 2, ..., M - 1. \tag{3.60}$$

At the boundaries,

$$\psi_1 = \hat{\psi}^-(z_1) \quad \text{and} \quad \psi_M = \hat{\psi}^+(z_M).$$

We use the ψ_i in (3.57), which will lead to equations for the positions of the plateau boundaries. The left hand side of (3.57) reduces to

$$\int_0^L \tilde{\varrho}_t \psi_i \, dx = \frac{1}{\varepsilon} \int_0^L \sum_{j=1}^M \left[-\dot{x}_j \hat{\varrho}_j'\left(\frac{x - x_j(t)}{\varepsilon}\right)\right] \psi_i \, dx$$

$$\sim -\frac{\dot{x}_i}{\varepsilon} \int_{\bar{x}_{i-1}}^{\bar{x}_i} \hat{\varrho}_i' \, dx = -\dot{x}_i \hat{\varrho}_i \Big|_{\frac{\bar{x}_{i-1}-x_i}{\varepsilon}}^{\frac{\bar{x}_i - x_i}{\varepsilon}} \sim \dot{x}_i(-1)^i.$$

We integrate by parts on the right hand side of (3.57). The boundary term from the first integral cancels with the last term in (3.57), and we obtain

$$\dot{x}_i(-1)^i \sim \int_0^L \psi_{i,x}\left(\tilde{\varrho}(1 - \tilde{\varrho})\tilde{S}_x - \varepsilon\tilde{\varrho}_x\right) dx. \tag{3.61}$$

In a first approximation, we can write the function $\psi_{i,x}$, $i = 2, ..., M - 1$ as the difference between two delta-distributions, $\psi_{i,x} \sim \delta(\bar{x}_{i-1}) - \delta(\bar{x}_i)$. Then, the right hand side of (3.61) can be evaluated at leading order by

$$\int_0^L \psi_{i,x} \tilde{\varrho}(1 - \tilde{\varrho})\tilde{S}_x \, dx \sim -\tilde{\varrho}(1 - \tilde{\varrho})\tilde{S}_x \Big|_{\bar{x}_{i-1}}^{\bar{x}_i},$$

$$-\int_0^L \varepsilon \psi_{i,x} \tilde{\varrho}_x \, dx \sim \varepsilon \left(\tilde{\varrho}_x(\bar{x}_i) - \tilde{\varrho}_x(\bar{x}_{i-1}) \right),$$

where, by the factor $\tilde{S}_x$, the first term is small compared to the second and will therefore be neglected. For further calculations we use

$$\varepsilon \tilde{\varrho}_x \sim \begin{cases} \hat{\varrho}_i' + \hat{\varrho}_{i-1}' & \text{at } x = \bar{x}_{i-1} \\ \hat{\varrho}_i' + \hat{\varrho}_{i+1}' & \text{at } x = \bar{x}_i. \end{cases}$$

Calculating the leading order terms using (3.44), we obtain a set of M coupled ODEs for the plateau boundaries x_i,

$$\dot{x}_1 \sim (-1)^{j+1} \left[S'(x_1) e^{(-1)^{j+1} S'(x_1) \frac{\bar{x}_1 - x_1}{\varepsilon}} + S'(x_2) e^{(-1)^{j+1} S'(x_2) \frac{\bar{x}_1 - x_2}{\varepsilon}} \right] \quad (3.62)$$

$$\begin{aligned} \dot{x}_i \sim (-1)^{i+j} \Big[& S'(x_i) e^{(-1)^{i+j} S'(x_i) \frac{\bar{x}_i - x_i}{\varepsilon}} + S'(x_{i+1}) e^{(-1)^{i+j} S'(x_{i+1}) \frac{\bar{x}_i - x_{i+1}}{\varepsilon}} \\ & - S'(x_i) e^{(-1)^{i+j-1} S'(x_i) \frac{\bar{x}_{i-1} - x_i}{\varepsilon}} - S'(x_{i-1}) e^{(-1)^{i+j-1} S'(x_{i-1}) \frac{\bar{x}_{i-1} - x_{i-1}}{\varepsilon}} \Big] \end{aligned} \quad (3.63)$$

for $i = 2, ..., M - 1$ and

$$\begin{aligned} \dot{x}_M \sim (-1)^{j+M-1} \Big[& S'(x_M) e^{(-1)^{j+M-1} S'(x_M) \frac{\bar{x}_{M-1} - x_M}{\varepsilon}} \\ & + S'(x_{M-1}) e^{(-1)^{j+M-1} S'(x_{M-1}) \frac{\bar{x}_{M-1} - x_{M-1}}{\varepsilon}} \Big], \end{aligned} \quad (3.64)$$

where $j = 1$ if the first plateau touches the boundary and $j = 0$ otherwise. Due to mass conservation, the equation

$$\sum_{i=1}^M (-1)^{i+j} \dot{x}_i = 0$$

holds. Therefore, only $M - 1$ equations are needed in order to determine the dynamics.

The whole asymptotic approach is based on the fact that the movement of the boundary layers is exponentially slow. It is valid only as long as all plateaus are spatially well separated and far from the boundaries, i.e.

$$|\bar{x}_i - x_i|, \ |\bar{x}_{i-1} - x_i| \gg \varepsilon, \quad i = 1, ..., M. \quad (3.65)$$
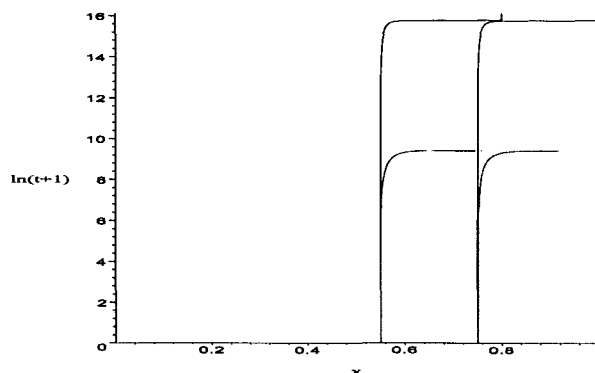
Figure 3.5: Comparison of the numerical solution of system (3.4), (3.5) with $\varepsilon = 2 \times 10^{-4}$ obtained with an upwind-scheme with grid size $\Delta x = \Delta t = 0.0012$ (light) and the numerical solution of the corresponding ODE-system (dark)

choose two different sets of initial conditions close to this stationary point and calculate the temporal evolution of the boundary layers according to (3.62) - (3.64) with $i = 4$. After a plateau has moved to the domain boundary or merged with the other plateau, we solve the system for $i = 3$ and $i = 2$ respectively.

In Fig. 3.6(a), the left plateau is initially closer to the boundary. The system passes relatively quickly into another pseudostationary state with two plateaus at the domain boundaries. The larger of the two plateaus attracts mass of the smaller one, until finally, the stable steady state of one plateau at the domain boundary is reached.

In Fig. 3.6(b), the left plateau is initially closer to the second plateau. Now, the plateaus merge first and then move towards the boundary. Dashed lines represent points where the asymptotic approach is no longer valid ($\dot{x}_1$, $\dot{x}_2 \approx \varepsilon$) and full solutions of (3.4), (3.5) have to be calculated. Fig. 3.7 shows the evolution of the cell density during this time interval. As the left plateau moves towards the right one, a rarefaction wave starts to form when the entropy condition for the corresponding hyperbolic system becomes violated. The outer plateau edge of the right plateau is not affected by this merging process and does not move, since locally, the entropy condition is still satisfied. As a consequence, it is sufficient to solve the equations for the plateau boundaries if one is only interested in the long-term dynamics of the parabolic system. If the dynamics of the coarsening process itself should be captured too, a hybrid numerical-asymptotic approach is the method of choice.
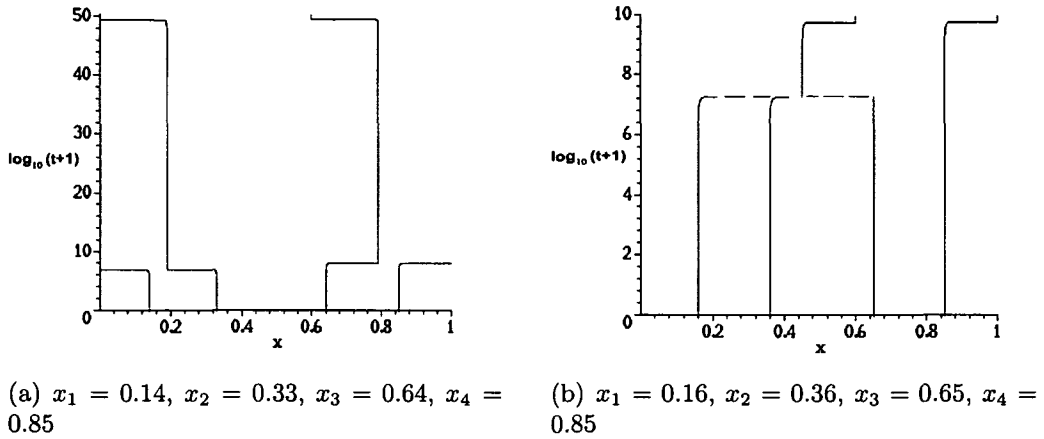
(a) $x_1 = 0.14$, $x_2 = 0.33$, $x_3 = 0.64$, $x_4 = 0.85$

(b) $x_1 = 0.16$, $x_2 = 0.36$, $x_3 = 0.65$, $x_4 = 0.85$

Figure 3.6: Solutions of the ODE-system (3.62) - (3.64) with different initial conditions and $\varepsilon = 2.7 \times 10^{-4}$.

(a) $t = 20379820$

(b) $t = 20379834$
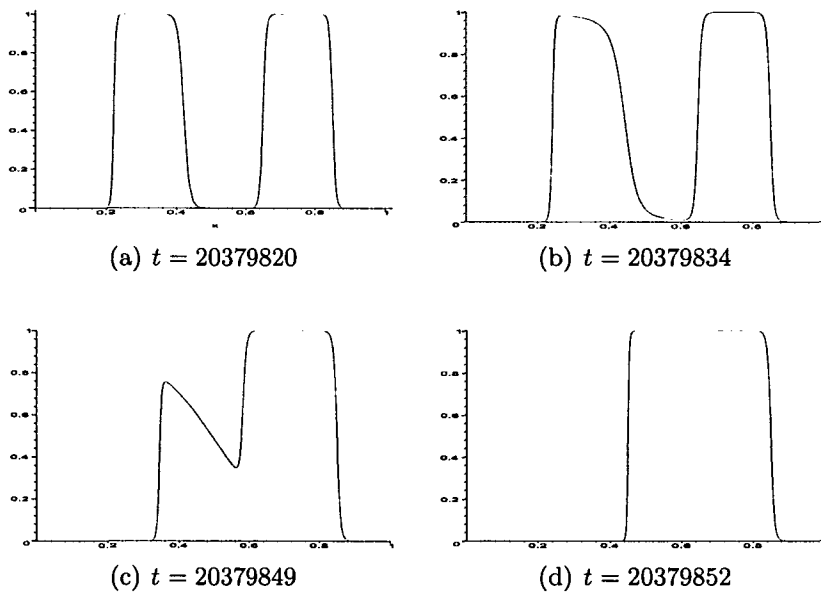
(c) $t = 20379849$

(d) $t = 20379852$

Figure 3.7: Fast dynamics of the parabolic system, corresponding to the dashed lines in Fig. 3.6(b). The first picture shows the cell density calculated according to the asymptotic approximations (3.62) - (3.64) and (3.45) shortly before the hyperbolic dynamics start to dominate. The middle pictures show a rarefaction wave obtained by solving (3.4), (3.5) with an upwind scheme until, as shown in the last picture, only one plateau is left.

Bibliography

[1] F. Alcantara and M. Monk. Signal propagation during aggregation in the slime mold *Dictyostelium discoideum*. *J. Gen. Microbiol.*, 85:321–334, 1974.

[2] W. Alt. Biased random walk models for chemotaxis and related diffusion approximations. *J. Math. Biol.*, 9(2):147–177, 1980.

[3] P. Bates and J. Xun. Metastable patterns for the Cahn-Hilliard equation I. *J. Differential Equations*, 2(111):421–457, 1994.

[4] P. Bates and J. Xun. Metastable patterns for the Cahn-Hilliard equation II. Layer dynamics and slow invariant manifold. *J. Differential Equations*, 1(117):165–216, 1995.

[5] C. Cattaneo. Sulla conduzione de calore. *Atti del Semin. Mat. e Fis. Univ. Modena*, 3:83–101, 1948.

[6] C. Cercignani. *Theory and Applications of the Boltzmann Equation.* Scottish Acad. Press, Edinburgh, 1975.

[7] F. Chalub, P. Markowich, B. Perthame, and C. Schmeiser. Kinetic models for chemotaxis and their drift-diffusion limits. *Monatsh. Math.*, 2004.

[8] J. Dallon and H.G. Othmer. A discrete cell model with adaptive signalling for aggregation of *Dictyostelium* aggregation. *Phil. Trans. R. Soc. Lond. B*, 352:391–417, 1997.

[9] Y. Dolak and T. Hillen. Cattaneo models for chemotaxis: Numerical solution and pattern formation. *J. Math. Biol.*, 46(2):153–170, 2002.

[10] F. Filbet, P. Laurencot, and B. Perthame. Derivation of hyperbolic models for chemosensitive movement. *submitted.*

[11] R. Firtel. http://www-biology.ucsd.edu/~firtel/movies.html.

[12] G.S. Fraenkel and D.L. Gunn. *The Orientation of Animals*. Dover Publ. inc. New York, 1961.

[13] J. Geiger, D. Wessels, and D. Soll. Human polymorphonuclear leukocytes respond to waves of chemoattractant, like *Dictyostelium*. *Cell Motil. Cytoskeleton*, 56:27–44, 2003.

[14] S. Goldstein. On diffusion by discontinuous movements and the telegraph equation. *Quart. J. Mech. Appl. Math.*, 4:129–156, 1951.

[15] K.P. Hadeler. Reaction transport equations in biological modeling. *Math. Comp. Model.*, 31:75–81, 2000.

[16] J. Haskovec and C. Schmeiser. Transport in semiconductors at saturated velocities. ANUM Preprint.

[17] T. Hillen. *Transport Equations and Chemosensitive Movement*. 2001. Habilitation thesis.

[18] T. Hillen. Transport equations with resting phases. *European J. Appl. Math.*, in print.

[19] T. Hillen. On the L^2-moment closure of transport equations: The Cattaneo approximation. *Discr. Cont. Dyn. Systems, Series B, 2004*, to appear.

[20] T. Hillen and H.G. Othmer. The diffusion limit of transport equations derived from velocity jump processes. *SIAM J. Appl. Math.*, 61(3):751–775, 2000.

[21] T. Hillen and K. Painter. Global existence for a parabolic chemotaxis model with prevention of overcrowding. *Adv. in Appl. Math.*, 26(4):280–301, 2001.

[22] T. Höfer, P.K. Maini, J.A. Sherratt, M. A. Chaplain, P. Chauvet, D. Metevier, P.C. Montes, and J.D. Murray. A resolution of the chemotactic wave paradox. *Appl. Math. Lett.*, 7(2):1–5, 1994.

[23] T. Höfer, J.A. Sherratt, and P.K. Maini. Cellular pattern formation during *Dictyostelium* aggregation. *Physica D*, 85:425–444, 1995.

[24] D. Horstmann. From 1970 until present: The Keller-Segel model in chemotaxis and its consequences, Part I. *Jahresbericht der DMV*, 105(3):103–165, 2003.

[25] D. Horstmann. From 1970 until present: The Keller-Segel model in chemotaxis and its consequences, Part II. *Jahresbericht der DMV*, to appear.

[26] M. Kac. A stochastic model related to the telegrapher's equation. *Rocky Mountain J. Math.*, 4:497–509, 1956.

[27] E.F. Keller and L.A. Segel. Initiation of slime mold aggregation viewed as an instability. *J. Theor. Biol.*, 26:399–415, 1970.

[28] J. Laforgue and R. O'Malley. Shock layer movement for Burgers' equation. *SIAM J. Appl. Math.*, 55(2):332–347, 1995.

[29] P.A. Markowich and P. Szmolyan. A system of convection-diffusion equations with small diffusion coefficient arising in semiconductor physics. *J. Differential Equations*, 81:234–254, 1989.

[30] J.L. Martiel and A. Goldbeter. A model based on receptor desensitization for cyclic AMP signalling in *Dictyostelium* cells. *Biophys. J.*, 52:807–828, 1987.

[31] P.C. Newell. *Fungal differentiation: A contemporary synthesis*, pages 43–71. Marcel Dekker, New York, 1983.

[32] H.G. Othmer and J. Dallon. A continuum analysis of the signal seen by *Dictyostelium discoideum*. *J. Theor. Biol.*, 194:61–483, 1998.

[33] H.G. Othmer, S.R. Dunbar, and W. Alt. Models of dispersal in biological systems. *J. Math. Biol.*, 26:263–298, 1988.

[34] H.G. Othmer and T. Hillen. The diffusion limit of transport equations II: Chemotaxis equations. *SIAM J. Appl. Math.*, 62(4):1222–1250, 2002.

[35] H.G. Othmer and P. Schaap. Oscillatory cAMP signaling in the development of *Dictyostelium discoideum*. *Comm. Theor. Biol.*, 5:175–282, 1998.

[36] K. Painter and T. Hillen. Volume-filling and quorum sensing in models for chemosensitive movement. *Canad. Appl. Math. Quart.*, 10(4):280–301, 2003.

[37] K. Painter, P. Maini, and H.G. Othmer. Stripe formation in juvenile pomacanthus via chemotactic response to a reaction-diffusion mechanism. *Proc. Natl. Acad. Sci. USA*, 96:5549–5554, 1999.

[38] K. Painter, P. Maini, and H.G. Othmer. A chemotactic model for the advance and retreat of the primitive streak in avian development. *Bull. Math. Biol.*, 62:501–525, 2000.

[39] C.V. Pao. *Nonlinear Parabolic and Elliptic equations*. Plenum Press, 1992.

[40] C.S. Patlak. Random walk with persistence and external bias. *Bull. Math. Biophys.*, 15:311–338, 1953.

[41] A.B. Potapov and T. Hillen. Metastability in chemotaxis models. *submitted.*

[42] F. Poupaud. Runaway phenomena and fluid approximation under high fields in semiconductor kinetic theory. *ZAMM Z. Angew. Math. Mech.*, 72(8):359–372, 1992.

[43] F. Poupaud and M. Rascle. Measure solutions to the linear multidimensional transport equation with non-smooth coefficients. *Comm. Partial Differential Equations*, 22(1-2):337–358, 1997.

[44] W.J. Rappel, P.J. Thomas, H. Levine, and W.F. Loomis. Establishing direction during chemotaxis in eukaryotic cells. *Biophysical J.*, 83:1361–1367, 2002.

[45] L. Reyna and M. Ward. On the exponentially slow motion of a viscous shock. *Comm. Pure Appl. Math.*, 48(2):79–120, 1995.

[46] M. Rivero, R. Tranquillo, H. Buettner, and D. Lauffenburger. Transport models for chemotactic cell populations based on individual cell behavior. *Chem. Eng. Sci.*, 44(12):2881–2897, 1989.

[47] J. Simon. Compact sets in the space $L^p(0, T; B)$. *Anal. Math. Pura Appl.*, 146:65–96, 1987.

[48] B. Sleeman, M. Ward, and J. Wei. Existence, stability and dynamics of spike patterns in a chemotaxis model. *in print.*

[49] D.R. Soll. Behavioral studies into the mechanism of eukaryotic chemotaxis. *J. Chem. Ecol.*, 16:133–150, 1990.

[50] D.R. Soll and D. Wessels. *Motion Analysis of Living Cells.* Wiley and Sons, New York, Toronto, 1998.

[51] D.W. Stroock. Some stochastic processes which arise from a model of the motion of a bacterium. *Probab. Theory and Related Fields*, 28:305–315, 1974.

[52] Y. Tang and H.G. Othmer. A G-protein based model of adaption in *Dictyostelium discoideum*. *Math. Biosci.*, 120:25–76, 1994.

[53] Y. Tang and H.G. Othmer. Excitation, oscillations and wave propagation in a G-protein based model of signal transduction in *Dictyostelium discoideum*. *Phil. Trans. R. Soc. Lond. B*, 349:179–195, 1995.

[54] B. Varnum, K. Edwards, and D.R. Soll. *Dictyostelium* amoebae alter motility differently in response to increasing versus decreasing temporal gradients in cAMP. *J. Cell Biol.*, 101:1–5, 1985.

[55] B. Varnum, K. Edwards, E. Voss, and D.R. Soll. Amebae of *Dictyostelium discoideum* respond to an increasing temporal gradient of the chemoattractant cAMP with a reduced frequency of turning: evidence for a temporal mechanism in amoeboid chemotaxis. *Cell Motil. Cytoskeleton*, 8:7–17, 1987.

[56] B. Varnum, E. Voss, and D.R. Soll. Frequency and orientation of pseudopod formation of *Dictyostelium discoideum* amoebae chemotaxing in a spatial gradient: further evidence for a temporal mechanism. *Cell Motil. Cytoskeleton*, 8:18–26, 1987.

[57] M. Ward. Exponential asymptotics and convection-diffusion-reaction models. *Analyzing Multiscale Phenomena Using Singular Perturbation Methods, Proceedings of Symposia in Applied Mathematics*, 56:151–184, 1998.

[58] D. Wessels, J. Murray, and D.R. Soll. Behaviour of *Dictyostelium* amoebae is regulated primarily by the temporal dynamics of the natural cAMP wave. *Cell Motil. Cytoskeleton*, 23:145–156, 1992.

Yasmin Dolak

Johann Radon Institute for Computational and Applied Mathematics
Austrian Academy of Sciences
Altenbergerstrasse 69, A-4040 Linz, Austria
yasmin.dolak@oeaw.ac.at

Personal Data

born on August, 8th 1977 in Vienna
Austrian citizen

Education

2001-2004	PhD in Applied mathematics at the Vienna University of Technology
	Title: Advection-dominated Models for Chemotaxis.
	Advisor: Dr. C. Schmeiser
2001	Diploma in Physics, Vienna University of Technology
	Diploma thesis at the Eberhard-Karls University in Tübingen, Germany
	Title: Simulation eines zweidimensionalen Cattaneosystems
	zur Beschreibung räumlicher Muster.
	Advisor: Dr. T. Hillen
1999/2000	Studies at the Université Paul Sabatier in Toulouse, France

Employment, Internships and Teaching Experience

09/04 - present	Research Scientist in the group "Partial Differential Equations" at the Johann Radon Institute (RICAM), Linz
10/02 - 06/03	Teaching assistant Vienna University of Technology
09/01 - 11/04	Student Member of the Wissenschaftskolleg "Differential Equation Models in Science and Engineering" supported by the Austrian Science Fund
10/00 - 02/01	Teaching assistant University Tübingen
07 - 09/99	Internship at the Université Laval, Canada (Computational nuclear physics)
04 - 06/98	Internship at the Centre Hospitalier Universitaire in Toulouse, France (Biophysics)
07 - 08/98	Internship at CERN, Switzerland (Theoretical physics)

Computational Skills

Programming languages: C, C++, FORTRAN
Operating Systems: Linux, Unix, Windows98+
Software: Maple, Latex, Word, Gnuplot, HTML etc.

Languages

German (native speaker)
English (fluently) ◇ French (fluently) ◇ Spanish (basic knowledge)

Publications

Y. Dolak and T. Hillen: Cattaneo Models for Chemotaxis: Numerical Solution and Pattern Formation. J. Math. Biol. 46 (2003) 2, 153-170.

Y. Dolak and C. Schmeiser: A kinetic theory approach to resolving the chemotactic wave paradox (Conference Proceeding). ESCULAPIO Pub. Co., Bologna, 2003

Y. Dolak and C. Schmeiser: Kinetic models for chemotaxis:
Hydrodynamic limits and the back-of-the-wave problem. ANUM Preprint 5/03.

Y. Dolak and C. Schmeiser: A Keller-Segel Model with small diffusivity.
ANUM Preprint 10/04.

Conference and Seminar Talks

09/2004	Centre for Mathematical Medicine, Nottingham, UK (Summer School for Cell adhesion and migration)
02/2004	IMPA, Rio de Janeiro (Workshop on Mathematical Biology and Evolutionary Dynamics)
12/2003:	Max-Planck Institute for Mathematics in the Sciences, Leipzig (Mathematical modeling of biological systems Seminar)
10/2003:	University of Cologne (Oberseminar Nichtlineare Analysis)
09/2003:	Meeting of the Austrian Mathematical Society in Bolzano, Italy
05/2003:	University of Maryland (Workshop on Analysis and Numerics) for Modeling Semiconductor Devices and Biological Channels)
05/2003:	Université de Nice Sophia-Antipolis, Nice (Journée "Modèles Mathematiques du chimiotactisme")
02/2003:	AMAM, Nice (Minisymposium Mathematical Models for Chemotaxis)
12/2002:	University of Alberta (Mathematical Biology Seminar)
07/2002:	ESMTB Conference in Milan (Minisymposium Individual and Population based models for chemosensitive movement)